Bhatt, S., D. J. Weiss, E. Cameron, D. Bisanzio, B. Mappin, U. Dalrymple, K. E. Battle, C. L. Moyes, A. Henry, P. A. Eckhoff, E. A. Wenger, O. Briet, M. A. Penny, T. A. Smith, A. Bennett, J. Yukich, T. P. Eisele, J. T. Griffin, C. A. Fergus, M. Lynch, F. Lindgren, J. M. Cohen, C. L. J. Murray, D. L. Smith, S. I. Hay, R. E. Cibulskis, and P. W. Gething. **The Effect of Malaria Control on Plasmodium Falciparum in Africa between 2000 and 2015**. *Nature* 526, no. 7572 (2015): 207-211.

http://dx.doi.org/10.1038/nature15535

The impact of malaria control on *Plasmodium falciparum* in Africa, 2000–2015

†$Bhatt, S.[1], †Weiss, D.J.[1], †Cameron, E.[1], Bisanzio, D.[1], Mappin, B.[1], Dalrymple, U.[1], Battle, K.[1], Moyes, C.L.[1], Henry, A.[1], Eckhoff, P.A.[2], Wenger, E.A.[2], Briët, O.[3, 4], Penny, M.A.[3, 4], Smith, T.A.[3, 4], Bennett, A.[5], Yukich, J.[6], Eisele, T.P.[6], Griffin, J.T.[7], Fergus, C.A.[8], Lynch, M.[8], Lindgren, F.[9], Murray, C.L.J.[10], Smith, D.L.[1, 11, 12], Hay, S.I.[10, 13, 14], Cibulskis, R.E.[8], $Gething, P.W.[1]

† These authors contributed equally

$ corresponding author

[1]*Spatial Ecology and Epidemiology Group, Tinbergen Building, Department of Zoology, University of Oxford, South Parks Road, Oxford, OX1 3PS, UK*

[2]*Institute for Disease Modeling, Intellectual Ventures, 1555 132nd Ave NE, Bellevue, WA 98005, USA*

[3]*Epidemiology and Public Health, Swiss Tropical and Public Health Institute, P.O. BOX 4002, Basel, Switzerland*

[4]*University of Basel, Petersplatz 1, P.O. BOX 4001, Basel, Switzerland*

[5]*Malaria Elimination Initiative, University of California San Francisco, 500 Parnassus Ave, San Francisco, CA 94143, San Francisco, USA*

[6]*Center for Applied Malaria Research and Evaluation, Tulane University School of Public Health and Tropical Medicine, 1440 Canal Street, Suite 2200 New Orleans, LA 70112, USA*

[7]*MRC Centre for Outbreak Analysis and Modelling, Department of Infectious Disease Epidemiology, Imperial College London, London, W2 1PG, UK*

[8]*Global Malaria Programme, World Health Organization, 20 Avenue Appia, 1211 Geneva 27, Switzerland*

[9]*Department of Mathematical Sciences, University of Bath, Claverton Down, Bath, BA2 7AY, UK*

[10]*Institute for Health Metrics and Evaluation, 2301 Fifth Ave., Suite 600, Seattle, WA 98121, USA*

[11]*Department of Epidemiology and Malaria Research Institute, John Hopkins Bloomberg School of Public Health, 615 North Wolfe Street , Baltimore, MD 21205, USA*

[12]*Sanaria Institute for Global Health and Tropical Medicine, Rockville, MD 20850, USA*

[13]*Wellcome Trust Centre for Human Genetics, University of Oxford, Oxford, OX3 7BN, UK*

[14]*Fogarty International Center, National Institutes of Health, Bethesda, MD 20892-2220, USA*

Since the turn of the millennium, a concerted international campaign against malaria has led to unprecedented levels of intervention coverage across sub-Saharan Africa. Understanding the impact of this control effort is vital to inform future policy decisions on the financing, planning, and implementation of post-2015 control efforts. However, the absence of reliable disease surveillance data, and the simplistic approaches underlying current estimates mean the impact of malaria interventions on transmission and disease burden across the varied epidemiological settings of Africa remains poorly understood. Here we present a Bayesian spatiotemporal modelling framework to link 27,573 malaria field surveys with detailed reconstructions of changing intervention coverage, directly evaluate trends from 2000–2015, and quantify the attributable effect of malaria disease control efforts. This provides an independent and data-driven assessment of progress made towards 2015 Millennium Development Goal (MDG) malaria targets. We found that *P. falciparum* infection prevalence in endemic Africa halved from 33 (95%CI: 30–35)% in 2000 to 16 (14–19)% in 2015. The incidence rate of clinical malaria declined by 40% over the same period from 321 (253–427) to 192 (135–265)/1000 per annum, with all but one of the 43 mainland endemic countries meeting the MDG target of reversing incidence trends by 2015, 19 achieving a >50% decline, and seven a > 75% decline. We estimate that interventions have averted 663 (542–753) million clinical cases since 2000, with insecticide treated nets by far the largest contributor (68% of cases averted). Despite coverage remaining well below target levels, current malaria intervention technologies have substantially reduced malaria disease incidence across the continent. Sustaining and increasing access to these interventions, as well as working to maintain their effectiveness in the face of insecticide and drug resistance, should form a cornerstone of post-2015 control strategies.

In the midst of an escalating malaria public health disaster, the year 2000 marked a turning point in multilateral commitment to malaria control in sub-Saharan Africa, catalysed by

the Roll Back Malaria initiative and the wider development agenda around the United Nations Millennium Development Goals (MDGs). The 15 years since have seen international financing for malaria control increase approximately twentyfold[1], enabling widespread but uneven scale-up of coverage of the main contemporary malaria control interventions: insecticide treated bednets (ITNs), indoor residual spraying (IRS), and prompt treatment of clinical malaria cases with artemisinin-based combination therapy (ACT).

As part of this reinvigorated effort, a series of international goals were set with a target year of 2015, in particular the MDG to "halt by 2015 and begin to reverse the incidence of malaria" and the more ambitious target defined later by the World Health Organization (WHO) of reducing case incidence by 75% relative to 2000 levels[3]. While these targets were important for motivating action and mobilising funds, no explicit plan was put in place to reliably measure progress towards them. Now that the benchmark year of 2015 has been reached, the international community must define a post-2015 agenda for malaria control that will shape the technical, financial, and political landscape in which the battle against the disease will be fought[4,5]. In this context, it is imperative that the 2015 achievements can be robustly evaluated and, more broadly, that the patterns, causes, and implications of changing malaria endemicity over the past 15 years can be understood to inform an optimal strategy for the future.

Despite its importance, current knowledge on the nature and drivers of changing endemicity in sub-Saharan Africa is remarkably weak. National health records in 32 highly endemic countries (together accounting for about 90% of the global malaria burden) are considered inadequate to assess trends in malaria cases[1]. For these countries, the WHO has previously adopted a "cartographic" burden measurement approach whereby a map of climatic suitability for malaria transmission is first used to stratify likely

incidence rates across the continent, with these rates then progressively downgraded as intervention coverage increases according to effect sizes measured in randomized control trials. One acknowledged limitation of this approach is its reliance on the central assumption that effects observed in a limited number of short-term trials can be extrapolated to sustained continent-wide implementation. This assumption has never been validated. In reality, the individual or combined efficacy of interventions will vary by setting and be contingent on many local factors including vector ecology, health systems and coverage levels[2,6]. Other studies have investigated effects using cross-sectional community surveys[6,7]. These studies capture a wider range of real-world settings, but yield only a single pooled estimate across diverse disease transmission settings that, again, has unknown validity when extrapolated across Africa.

Since its first use, component parts of the cartographic burden framework have incrementally improved. Climatic suitability maps have been superseded by empirical endemicity maps[8–10] that use model-based geostatistics to create surfaces of risk based on thousands of geolocated cross-sectional surveys measuring infection prevalence (termed *Plasmodium falciparum* parasite rate, *Pf*PR). Improvements have also been made in the estimation of clinical incidence rates from *Pf*PR[11–13] which allows the former quantity, which is notoriously difficult to measure in the field, to be estimated geographically using mapped surfaces of the latter[12,14]. All these earlier studies, however, preceded the most intense period of control effort (from 2010 to the present) and none were designed to formally evaluate temporal changes in disease burden or explicitly consider the impact of interventions.

Here, we provide the first formal quantification, with robustly defined uncertainty, of *P. falciparum* infection prevalence and disease incidence across sub-Saharan Africa

from the year 2000 to the benchmark year of 2015, and of the role the major control interventions have had in causing these changes.

Data on ITN use and access to ACTs from over one million households were combined with national malaria control programme data[1] on ITN, ACT, and IRS provision to develop time-series models of coverage of these interventions within each country[1]. These were combined within a spatiotemporal Bayesian geostatistical model[15] with *Pf*PR data from 27,573 georeferenced population clusters between 1995 and 2014, along with an optimised suite of temporally dynamic environmental and sociodemographic covariates[16]. The model adjusted *Pf*PR observations by age[17], season, and type of diagnostic used, and fitted flexible functional forms to capture the effect of each intervention on declining *Pf*PR as a function of coverage reached and the starting (pre-intervention) *Pf*PR in 2000. The model was used to predict a spatio-temporal "cube" of age-structured *Pf*PR at 5×5 km resolution across all endemic African countries for each year from 2000 to 2015. Using the empirically observed effect of each intervention, it was possible to generate counterfactual maps estimating contemporary *Pf*PR under hypothetical scenarios without interventions.

For the 32 high-burden countries of Africa, an ensemble model was developed to predict rates of clinical disease as a function of community *Pf*PR[18]. This brought together three independently developed mathematical malaria transmission models[12,13,19] that were re-fitted to a common dataset of age-structured clinical incidence measured longitudinally at 30 sites[20], allowing an ensemble model to be defined to predict age-specific incidence at all locations given prevalence, seasonality, level of treatment, and likely immune status of populations. This ensemble model was then combined with the *Pf*PR cube and underlying population surfaces[21] to predict clinical incidence by country and year for both the real and counterfactual scenarios. For the remaining eleven low-burden countries in Africa

(accounting for around 3% of cases) where national reporting systems are more robust, we generated clinical incidence estimates with an existing approach that uses national case reports while adjusting for care-seeking behaviour, low diagnostic testing rates, and underreporting[1,22].

We found that infection prevalence in children age 2-up-to-10 across endemic Africa has halved since the year 2000 (population-weighted mean *Pf*PR_{2-10}: year 2000 = 33%, 95% credible interval 31–35%; year 2015 = 16%, 14–19%), with around three-quarters of this decline occurring after 2005. Our predicted surfaces of *Pf*PR_{2-10} demonstrate the geographical pattern of this reduction across the continent (Figure 1a, b, c), with hyper- or holo-endemic transmission (*Pf*PR > 50%) common in 2000 across large swathes of central and western Africa but limited to isolated pockets by 2015. This decline meant a marked shift in the distribution of exposure level (Figure 1d), with the proportion of the endemic population exposed to hyper- or holo-endemic malaria falling from 33% to just 9% (Table 1). Crucially, for the feasibility of post-2015 elimination efforts, the population of stable endemic Africa experiencing very low transmission (*Pf* PR_{2-10} less than 1%) has increased six-fold since 2000 (far outstripping the 50% underlying population growth over the period) meaning there are now 121 million people living in settings where elimination campaigns can be launched.

We estimated that there were 187 (132–259) million clinical cases of *P. falciparum* malaria in Africa in 2015. Case incidence declined by 40% from 321 (253–427)/1000 per annum in 2000 to 192 (135–265)/1000 p.a. in 2015, with all but one of the 43 mainland endemic countries meeting the MDG target of reversing incidence trends by 2015, 19 achieving a >50% decline, and seven declining by > 75% (Extended Data Figure 3).

Changes in prevalence largely followed patterns of increasing ITN coverage, and ITNs were by far the most important intervention across Africa, accounting for an

estimated 68% of the declines in *Pf*PR seen by 2015 (Figure 2a). We estimated ACT and IRS contributed 19% and 13% respectively, although these interventions had larger proportional contributions where their coverage was high (Extended Data Figure 2). In total, we estimated that malaria control interventions have averted 663 (542–753) million clinical cases since 2000, of which 68%, 22% and 10% were contributed by ITNs, ACTs, and IRS, respectively (Figure 2b).

The results presented here are the first time the rapidly changing landscape of malaria risk in Africa has been quantified across the 15-year span of the Millennium Development Goals, driven primarily by empirical observations in the field rather than theoretical models or extrapolated experimental results. Our modelling framework requires few prior assumptions and allows patterns of change and attribution to be identified with robust accompanying metrics of uncertainty.

We have shown that dramatic and widespread reductions in infection prevalence and case incidence have occurred across Africa since 2000, and that malaria control interventions have been responsible for most of the decline even though they remain well below international targets for universal coverage[1]. ITNs have had by far the largest impact, but have also been generally present for longer and at higher levels of coverage. IRS and ACTs have both made important contributions to reducing prevalence and incidence where they have been implemented at scale (although it is important to note that the primary role of ACTs is in averting severe disease and death rather than reducing transmission and uncomplicated cases).

The efforts of the international community over the past 15 years have reduced malaria risk levels for many millions of people, and large regions of Africa are now in a position to consider elimination strategies. This analysis demonstrates that current malaria interventions have been highly effective at reducing prevalence and incidence across the

continent, and provides strong support for sustaining and increasing access to these interventions as a cornerstone of post-2015 control strategies.

Supplementary Information is linked to the online version of the paper at www.nature.com/nature.

Acknowledgements The authors acknowledge assistance from Melanie Renshaw in providing information from the Roll Back Malaria Harmonization Working Group Programmatic Gap Analysis and other guidance in the interpretation of our results. We thank members of the Roll Back Malaria Monitoring and Evaluation Reference Group (RBM-MERG) and the World Health Organization Surveillance Monitoring and Evaluation Technical expert Group (SME-TEG) for their feedback and suggestions. We thank Clara Burgert of the DHS Program for her assistance with DHS Survey access and interpretation. PWG is a Career Development Fellow (#K00669X) jointly funded by the UK Medical Research Council (MRC) and the UK Department for International Development (DFID) under the MRC/DFID Concordat agreement and receives support from the Bill and Melinda Gates Foundation (#OPP1068048, #OPP1106023). These grants also support EC, SB, BM, UD, DJW, DB, and AH. The Swiss TPH component was supported through the project #OPP1032350 funded by the Bill and Melinda Gates Foundation (BMGF). SIH is funded by a Senior Research Fellowship from the Wellcome Trust (#095066), which also supports KEB, and a grant from the Bill & Melinda Gates Foundation (#OPP1119467). He also acknowledges funding support from the RAPIDD program of the Science & Technology Directorate, Department of Homeland Security, and the Fogarty International Center, National Institutes of Health. JTG is funded by an MRC Fellowship (#G1002284). EAW and PAE are funded by the Global Good Fund.

Author Contributions Conceived of and designed the research: PWG and SB. Drafted the manuscript: PWG and SB. Drafted the supplementary information: SB, DJW, EC, DB, UD, BM. Prepared data: DJW, BM, UD, KB, CLM, AH, AB,JY,TPE. Conducted the analyses: SB, DJW, EC, DB, CAF, ML, REC. Supported the analyses: KB, PAE, EAW,

OB, MAP, TAS, JTG, CAF, ML, FL, DLS. Supported interpretation and policy contextualization: AB, TPE, JY, CAF, ML, CLJM, DLS, SIH, REC, PWG. All authors discussed the results and contributed to the revision of the final manuscript.

Author Information Reprints and permission information is available at www.nature.com/reprints. Correspondence and requests for materials should be addressed to PWG (peter.gething@zoo.ox.ac.uk).

Tables

Table 1 | Changing distribution of malaria endemicity across stable endemic Africa, 2000 to 2015

	Population (%)			Area (%)		
Endemicity class	**2000**	**2015**	**Change (%)**	**2000**	**2015**	**Change (%)**
Holo (*Pf*PR_{2-10} ≥75%)	11.57	1.32	-88.57	11.81	1.38	-88.32
Hyper (*Pf*PR_{2-10} 50–75%)	21.51	7.46	-65.31	20.18	7.88	-60.93
Meso (*Pf*PR_{2-10} 10–50%)	41.32	42.41	+2.64	40.98	41.06	+0.19
Hypo (*Pf*PR_{2-10} <10%)	25.60	48.80	+90.63	27.02	49.67	+83.84
Total	*100.00*	*100.00*		*100.00*	*100.00*	
Pre-elimination or eliminating (*Pf*PR_{2-10}<1%)	3.82	13.61	+255.93	3.48	11.39	+227.51

Figures

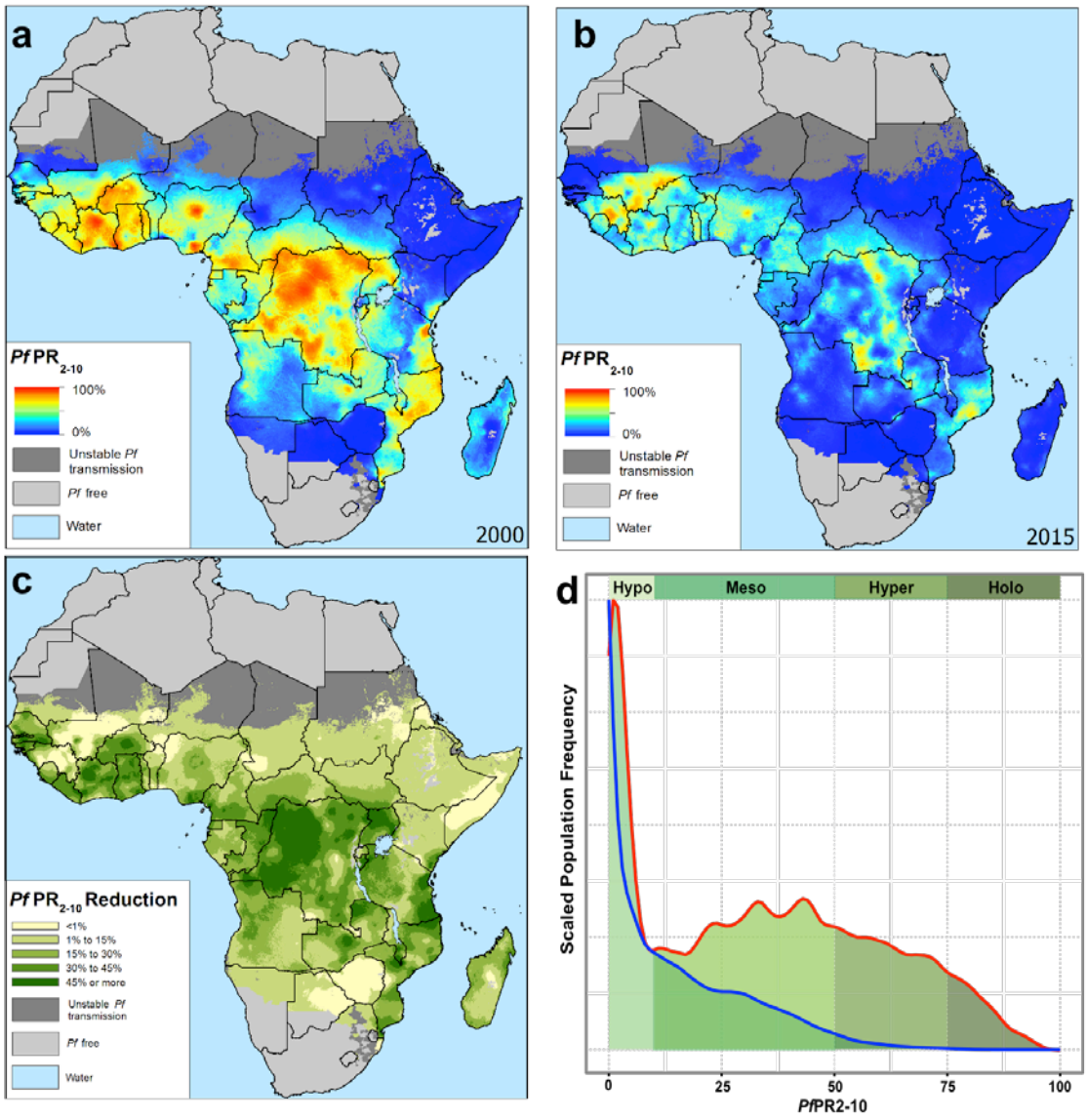

Figure 1 | Changes in infection prevalence 2000–2015. a, *Pf*PR$_{2\text{-}10}$ for the year 2000 predicted at 5×5 km resolution. **b,** *Pf*PR$_{2\text{-}10}$ for the year 2015 predicted at 5×5 km resolution. **c,** absolute reduction in *Pf*PR$_{2\text{-}10}$ from 2000 to 2015. **d,** smoothed density plot showing the relative distribution of endemic populations by *Pf*PR$_{2\text{-}10}$ in the years 2000 (red line) and 2015 (blue line). The frequencies on the vertical axis have been scaled to make the densities visually comparable. The classical endemicity categories are shown for reference in green shades.

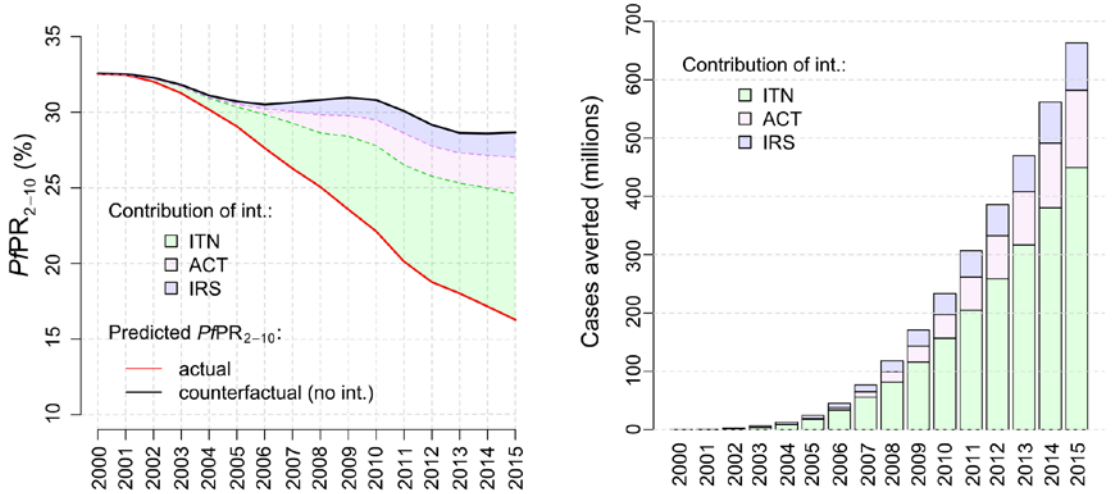

Figure 2 | Changing endemicity and impact of interventions 2000–2015. a, predicted time series of population-weighted mean *Pf*PR$_{2\text{-}10}$ across endemic Africa. The red line shows the actual prediction and the black line a 'counterfactual' prediction in a scenario without coverage by ITNs, ACTs, or IRS. The coloured regions indicate the relative contribution of each intervention in reducing *Pf*PR$_{2\text{-}10}$ throughout the period. **b,** the predicted cumulative number of clinical cases averted by interventions at the end of each year, with the specific contribution of each intervention distinguished.

Methods

***Pf*PR surveys.** To map endemicity (defined by the *P. falciparum* parasite rate, *Pf*PR) within boundaries of stable transmission, we added data points to the existing Malaria Atlas Project *Pf*PR database[9] via systematic literature searches from published data sources, direct communications with malaria specialists, and by incorporating data from 28 cross-sectional household surveys conducted in African countries since 2010. In total, we used 27,573 high fidelity geopositioned cluster level points spanning a temporal range from 1995 to 2014. Data were available for 53.3% of country years included in our analysis. All *Pf*PR points were processed to ensure accurate geopositioning, corrected for diagnostic type and age standardised to the epidemiologically relevant 2–10 years age range[17].

Environmental and socioeconomic covariates. The covariates used in our analysis consisted of temporally dynamic raster layers spanning all of Africa at a 5×5 km spatial resolution. These covariates comprised a mixture of environmental variables (e.g. vegetation indices), biological model variables (e.g. temperature suitability[23]), and socioeconomic variables (e.g. night time lights). A variable selection procedure was performed by first identifying, through an exhaustive literature review, a base set of biologically relevant variables that could be used in *Pf*PR mapping. By changing spatial and temporal lags, applying non-linear transformations, and including bivariate interactions we expanded the base set of covariates to a set of more than 55 million candidate variables, from which a rigorous statistical selection procedure identified 20 predictive covariates[16]. As our analysis spanned the years 2000 to 2015, but our covariates only covered 2000 to 2014, we projected values of covariates for 2015 as an average of years 2012, 2013 and 2014.

Interventions. Coverage of the three primary malaria control interventions was incorporated in our analysis: (a) insecticide treated bed nets (ITNs, λ), (b) indoor residual spraying (IRS, δ), and (c) artemisinin based combination therapy (ACT, η).

To derive estimates for ITN coverage (proportion of individuals that slept under a net the previous night) through time we first estimated national-level timeseries of ITN access (% population with access to an ITN in their household) using a Bayesian compartmental model that triangulated data on ITN manufacturer deliveries and ITN distribution programmes within countries with national cross-sectional survey data on ITN access within households. To predict within-country variation, we used a latent Gaussian model (LGM)[24] on the cross-sectional household survey data comprising over 600,000 households and 24,868 unique geopositioned cluster points, with the national-level time-series used to detrend the LGM. The data on ITN access spanned years 2000 to 2014, and for 2015 we used data from the Roll Back Malaria Harmonization Working Group gap analysis exercise[25] on projected commodity financing as a plausible estimate of future intervention levels relative to 2014. We then used a second LGM to generate a 5×5 km spatiotemporal prediction of the proportional difference between ITN access and ITN use (the "use gap"[26]) from the survey data. Finally, by multiplying the predicted ITN access and the complement of the use gap cubes we generated a third cube of predicted ITN use, again at 5×5 km resolution and spanning years 2000–2015.

IRS data were obtained at the national level directly from WHO country reporting as the proportion of the population protected by IRS campaigns each year[1]. These data were complete and covered years 2000–2013, although have acknowledged limitations due to inconsistent interpretation and reporting between countries. Data for years 2014 and 2015 were estimated as the average over 2011, 2012 and 2013.

To represent ACT coverage, we assembled data from 96 cross-sectional household surveys in 43 countries collected between 2004 to 2015. These surveys reported the proportion of febrile children over a 14-day recall period who accessed an ACT, and we used this indicator directly while acknowledging it does not capture poor adherence to treatment or drug efficacy. For those country-years where no survey was available, we built a predictive model that incorporated complete national-level data on annual ACTs distributed per capita (a proxy for drug availability). An LGM was used to build a predictive relationship between the two types of data, allowing treatment rates to be predicted continuously through time for all countries. Our LGM included temporal smoothing and country and regional level random effects embedded within a jack-knife approach that allowed us to generate appropriate uncertainty bounds.

Modelling of *Pf*PR. Each parasite rate observation was age- and diagnostic-adjusted and defined both spatially (*s*) and temporally (*t*) with co-located environmental and socioeconomic covariates ($X_{s,t}$) and intervention coverage levels ($\mathcal{I}_{s,t}$). We split our data into two subsets: a "pre-intervention" subset, consisting of 4,757 *Pf*PR geopositioned cluster points from country-years where national-level coverage from all three interventions remained at negligible levels, and a "post-intervention" subset for the remaining 22,816 cluster points. We used the pre-intervention data in an LGM to determine a 5×5 km surface of predicted "baseline" parasite rate ($\mathcal{B}_s$), representing $Pf\mathrm{PR}_{2\text{-}10}$ levels in conditions without ITNs, IRS or ACTs. This baseline allowed us to model change in parasite rate through time by the measurement equation:

$$PfPR_{s,t,2-10} \sim \beta X_{s,t} + \alpha \mathcal{I}_{s,t} + \gamma \mathcal{B}_s + Z_{s,t} + Y_c + \epsilon.$$

where β, α, γ are coefficients, $Z_{s,t}$ is a Gauss Markov random spatio-temporal field[24] with Matérn spatial and autoregressive temporal dynamics, Y_c are country (c) specific random effects, and ϵ is residual Gaussian variation. Conceptually this equation represents a model where, given no changes induced by environmental, socioeconomic, intervention related or residual unobserved correlated effects, the parasite rate at any point in time should be equal to the stable baseline parasite rate. Interventions $\mathcal{I}_{s,t} \in [\lambda_{trans}, \delta_{lag}, \eta_{lag}]$, with λ representing ITNs, δ representing IRS, and η representing ACTs, were also transformed from their raw data by setting δ_{lag} and η_{lag} as a moving average with a 2-year lag, thereby approximating the residual effect of interventions year to year. Following from well established mechanistic models on ITN effects[12,27,28] , λ was transformed as a four-year moving average (λ_{avg}) and allowed to interact with the baseline parasite rate through the non-linear function $\lambda_{trans} = (\mathcal{B}_s^a - \mathcal{B}_s^b){\lambda_{avg}}^{c\mathcal{B}_s}$, were a, b and c are coefficients. This nonlinear form was empirically derived from a large suite of candidate functions that replicated quantitative and qualitative forms described in the mechanistic models (Extended Data Figure 4). Fitting of the posterior LGM was achieved using Laplace approximations, and conditional realisations were simulated from the closed form conditional posterior.

Ensemble model for clinical incidence. There is no firm consensus on the form of the relationship between *Pf*PR and rates of clinical incidence in a given population. To define this relationship for use in our model, we developed an ensemble modelling approach that constrained the prevalence-incidence relationship while spanning the plausible range of both conceptual and empirical uncertainty with a combination of three contemporary micro-simulation codes: OpenMalaria[13,27], the EMOD DTK[19,29], and a version of the Griffin *et al*. model[12,30] which were refitted to a common dataset based on an exhaustive

literature search for studies reporting active case detection data[20]. Age-, seasonality-, and treatment-structured prevalence-incidence curves were drawn from the posterior predictive distributions of each model and combined into a single ensemble model using a weighting scheme based on the M-posteriors algorithm. Rates of clinical incidence were then estimated for each 5×5 km pixel by direct simulation from the posterior predictive distribution of $Pf\mathrm{PR}_{s,t,2-10}$ propagated through the posterior distribution of the ensemble model, and combined with an age-structured population denominator from the WorldPop[21] population product.

References

1. World Health Organization. *World Malaria Report 2014*. (World Health Organization, Geneva, 2014).
2. Lengeler, C. Insecticide-treated bed nets and curtains for preventing malaria. *Cochrane database Syst. Rev.* CD000363 (2004).
3. Roll Back Malaria Partnership/World Health Organization. *Global Malaria Action Plan 1 (2000-2015)*. (World Health Organization, Geneva, 2008).
4. Roll Back Malaria Partnership/World Health Organization. *Global Malaria Action Plan 2 (2016-2030)*. (World Health Organization, Geneva, 2015).
5. World Health Organization. *Draft Global Technical Strategy for Malaria 2016–2030*. (World Health Organization, Geneva, 2014).
6. Lim, S. S. *et al.* Net benefits: a multicountry analysis of observational data examining associations between insecticide-treated mosquito nets and health outcomes. *PLoS Med.* **8,** e1001091 (2011).
7. Giardina, F. *et al.* Effects of vector-control interventions on changes in risk of malaria parasitaemia in sub-Saharan Africa: a spatial and temporal analysis. *Lancet Glob. Heal.* **2,** e601–e615 (2014).
8. Hay, S. I. *et al.* A world malaria map: *Plasmodium falciparum* endemicity in 2007. *PLoS Med.* **6,** e1000048 (2009).
9. Gething, P. W. *et al.* A new world malaria map: *Plasmodium falciparum* endemicity in 2010. *Malar. J.* **10,** 378 (2011).
10. Noor, A. M. *et al.* The changing risk of *Plasmodium falciparum* malaria infection in Africa: 2000-10: a spatial and temporal analysis of transmission intensity. *Lancet* **383,** 1739–47 (2014).
11. Patil, A. P. *et al.* Defining the relationship between *Plasmodium falciparum* parasite rate and clinical disease: statistical models for disease burden estimation. *Malar. J.* **8,** 186 (2009).
12. Griffin, J. T., Ferguson, N. M. & Ghani, A. C. Estimates of the changing age-burden of Plasmodium falciparum malaria disease in sub-Saharan Africa. *Nat. Commun.* **5,** 3136 (2014).
13. Smith, T. *et al.* Ensemble modeling of the likely public health impact of a pre-erythrocytic malaria vaccine. *PLoS Med.* **9,** e1001157 (2012).
14. Hay, S. I. *et al.* Estimating the global clinical burden of *Plasmodium falciparum* malaria in 2007. *PLoS Med.* **7,** 14 (2010).
15. Diggle, P. & Ribeiro, P. *Model-based Geostatistics*. (Springer, New York, 2007).
16. Weiss, D. J. *et al.* Re-examining environmental correlates of *Plasmodium falciparum* malaria endemicity: a data-intensive variable selection approach. *Malar. J.* **14,** 68 (2015).
17. Smith, D. L., Guerra, C. A., Snow, R. W. & Hay, S. I. Standardizing estimates of the *Plasmodium falciparum* parasite rate. *Malar. J.* **6,** 131 (2007).
18. Cameron, E. *et al.* Defining the relationship between infection prevalence and clinical incidence of *Plasmodium falciparum* malaria. *Nat. Commun.*
19. Wenger, E. A. & Eckhoff, P. A. A mathematical model of the impact of present and future malaria vaccines. *Malar J* **12,** 10 (2013).

20. Battle, K. E. *et al.* Global database of *Plasmodium falciparum* and *P.vivax* incidence records. *Sci. Data*

21. WorldPop. *WorldPop gridded population distributions*. (www.worldpop.org.uk, 2015).

22. Cibulskis, R. E., Aregawi, M., Williams, R., Otten, M. & Dye, C. Worldwide incidence of malaria in 2009: estimates, time trends, and a critique of methods. *PLoS Med.* **8,** e1001142 (2011).

23. Weiss, D. J. *et al.* Air temperature suitability for *Plasmodium falciparum* malaria transmission in Africa 2000-2012: a high-resolution spatiotemporal prediction. *Malar. J.* **13,** 171 (2014).

24. Lindgren, F., Rue, H. & Lindström, J. An explicit link between Gaussian fields and Gaussian Markov random fields: The SPDE approach. *J. R. Stat. Soc. Ser. B* **73,** 423–498 (2011).

25. Roll Back Malaria Partnership Harmonization Working Group. *Programmatic Gap Analysis.* (http://www.rollbackmalaria.org/toolbox/tool_ProgrammaticGapAnalysis.html., 2014).

26. Kilian, A. *et al.* Universal coverage with insecticide-treated nets - applying the revised indicators for ownership and use to the Nigeria 2010 malaria indicator survey data. *Malar. J.* **12,** 314 (2013).

27. Smith, T. *et al.* Mathematical modeling of the impact of malaria vaccines on the clinical epidemiology and natural history of *Plasmodium falciparum* malaria: Overview. *Am. J. Trop. Med. Hyg.* **75,** 1–10 (2006).

28. Smith, D. L., Hay, S. I., Noor, A. M. & Snow, R. W. Predicting changing malaria risk after expanded insecticide-treated net coverage in Africa. *Trends Parasitol.* **25,** 511–516 (2009).

29. Eckhoff, P. A. A malaria transmission-directed model of mosquito life cycle and ecology. *Malar J* **10,** 1 (2011).

30. Griffin, J. T. *et al.* Reducing *Plasmodium falciparum* malaria transmission in Africa: a model-based evaluation of intervention strategies. *PLoS Med.* **7,** e1000324 (2010).

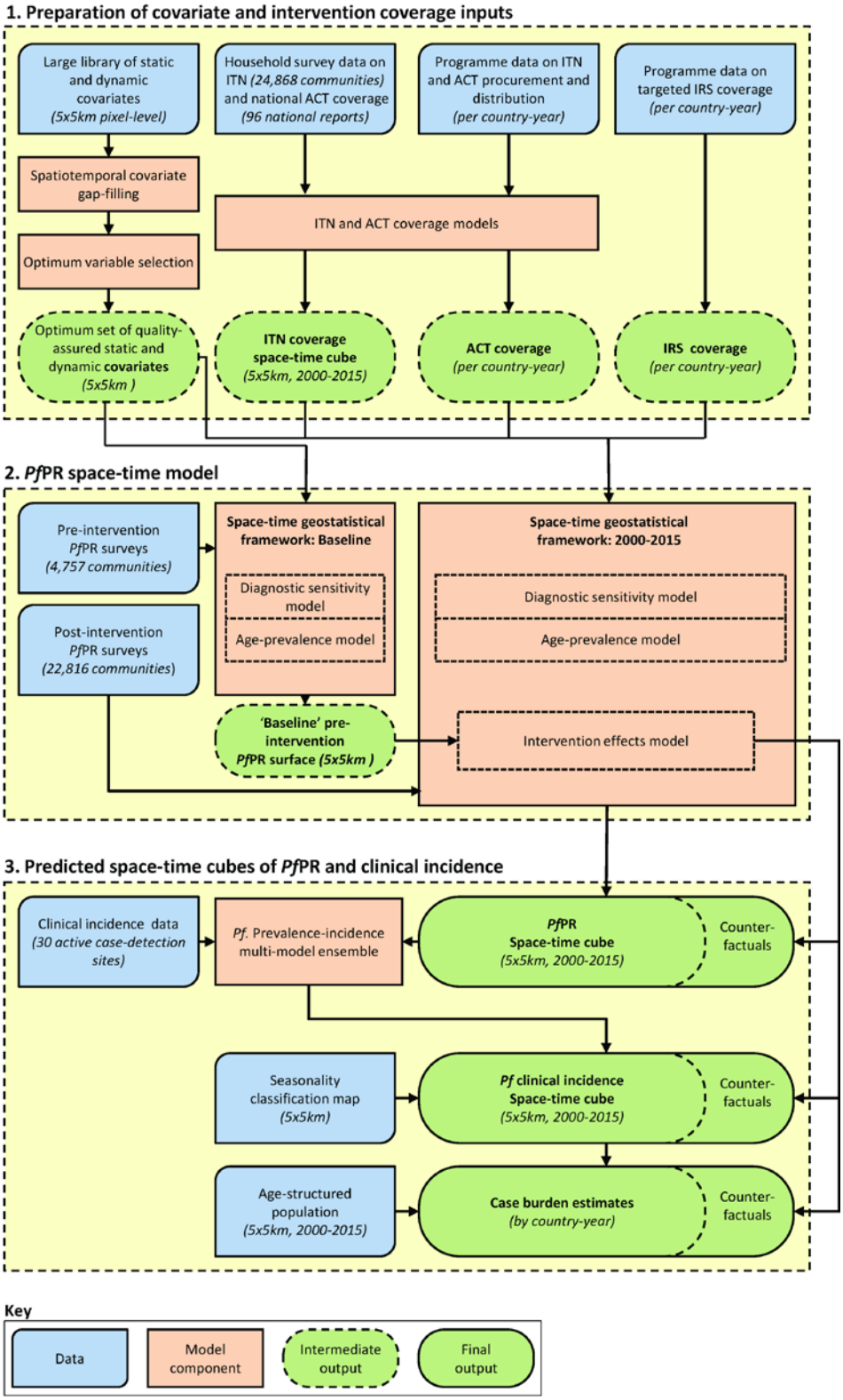

Extended Data Figure 1 | Schematic overview of main input data, model components, and outputs. Each component is summarised in the Methods and detailed in the Supplementary Information.

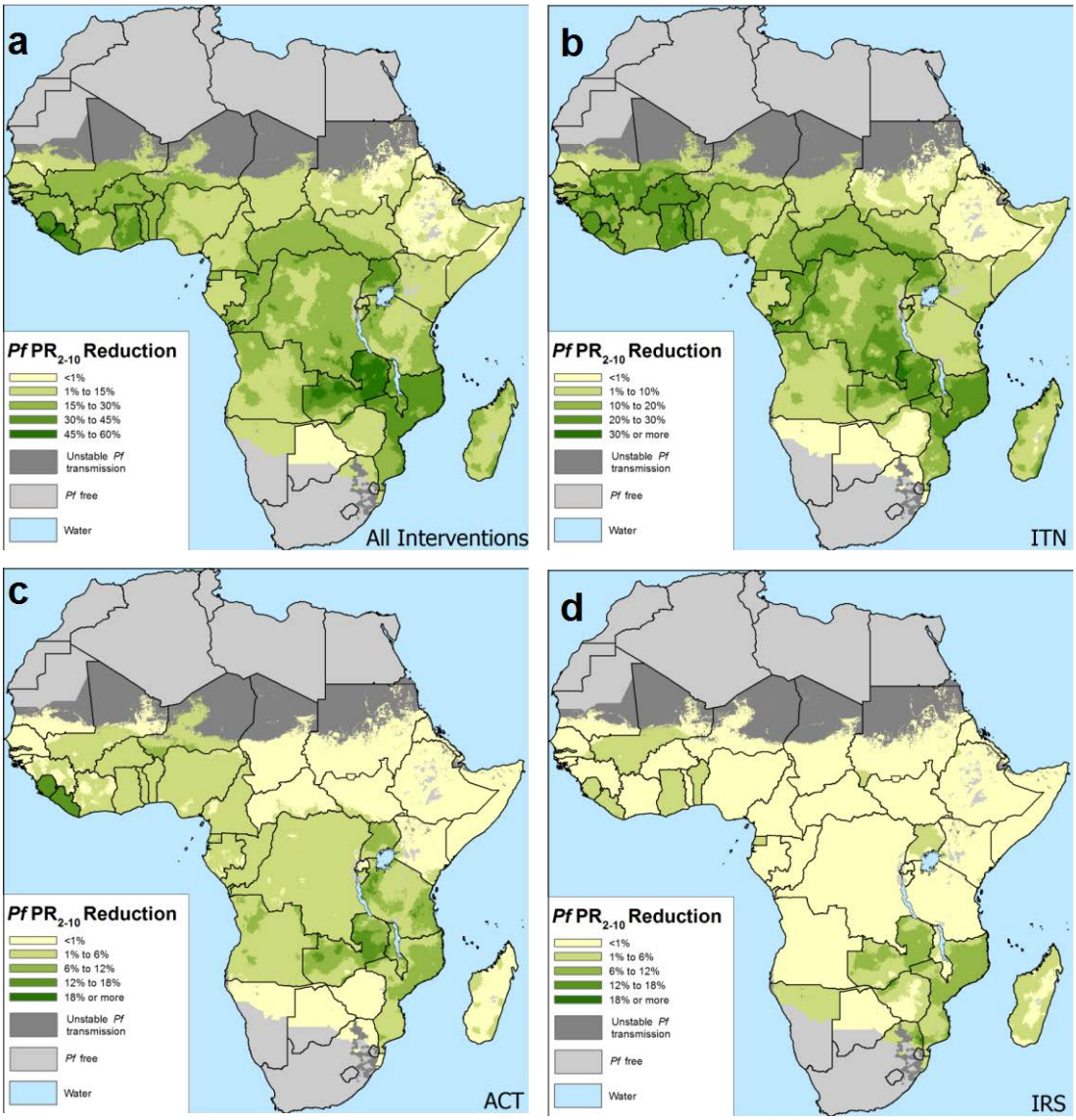

Extended Data Figure 2 | Decline in infection prevalence attributable to main malaria control interventions. Each map shows absolute decline in *Pf*PR_{2-10} between 2000 and 2015 within areas of stable transmission attributable to **a,** the combined impact of ITNs, ACTs, and IRS; the individual impact of **b,** ITNs**; c,** ACTs**; d,** IRS.

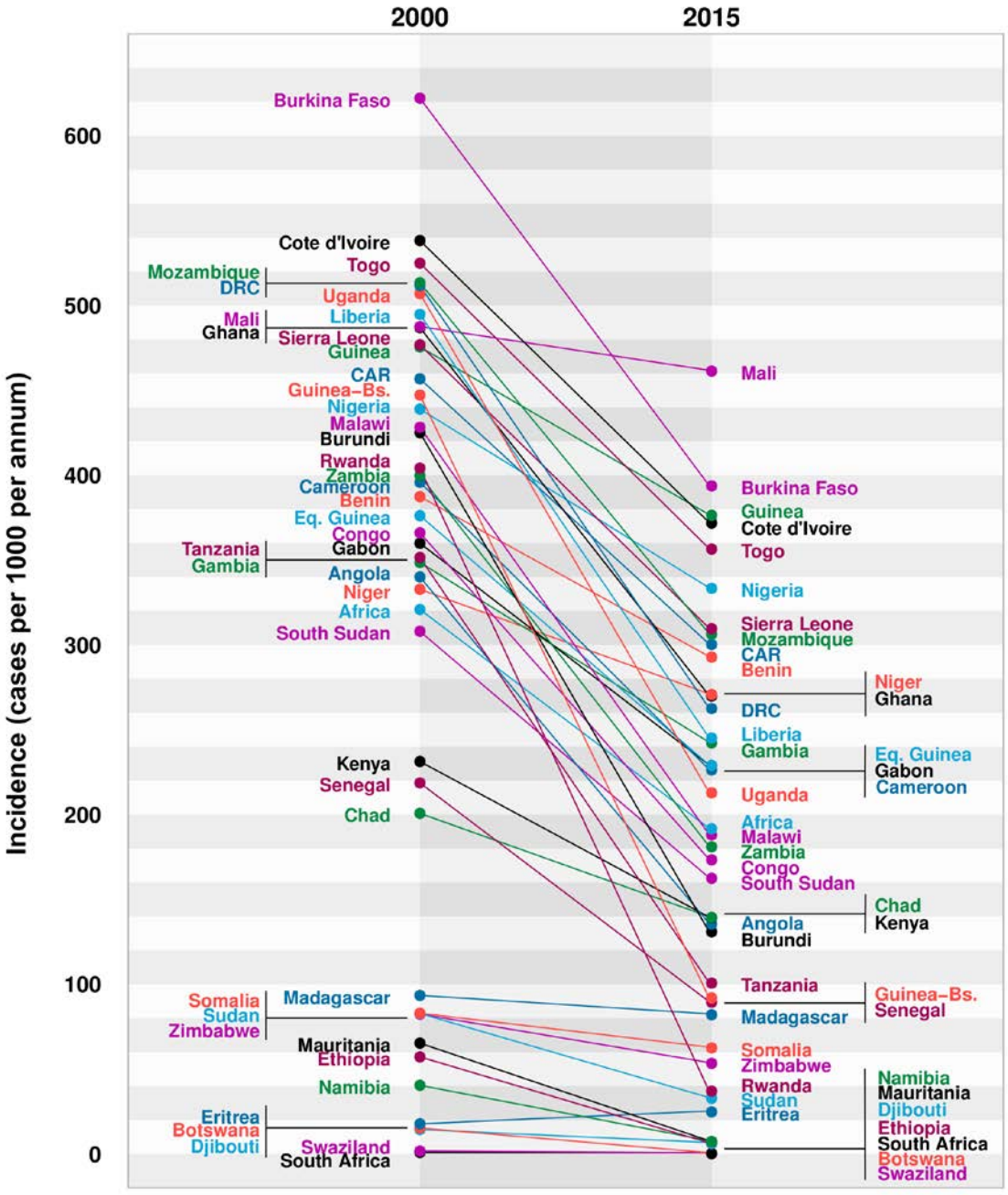

Extended Data Figure 3 | Changing incidence rate by country, 2000–2015.

Estimated country-level rates of all-age clinical incidence are shown for 2000 and 2015. For Sudan and South Sudan, we used the post-2011 borders throughout the time period to allow comparability.

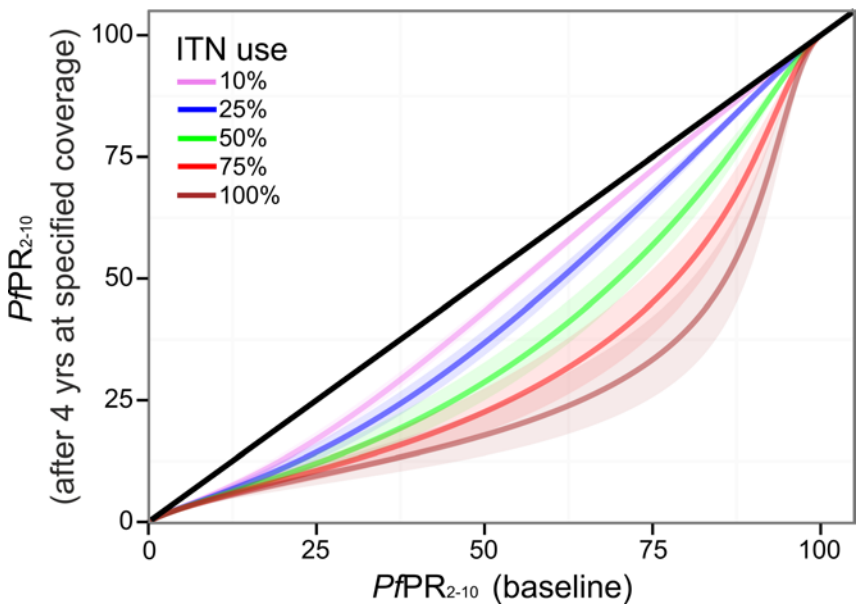

Extended Data Figure 4 | Fitted function representing impact of ITNs. Curves illustrate the predicted impact of ITNs as a function of coverage (five example coverage levels are shown, specified as mean coverage over preceding 4-year period) and baseline transmission. The baseline *Pf*PR is shown on the horizontal axis and the suppressed *Pf*PR given the ITN coverage level shown on the vertical axis. The diagonal line (representing zero ITN impact) is shown in black, and parameter uncertainty around each ITN impact line is illustrated by the semi-transparent envelopes.

Supplementary Information

Contents

1.0 OUTLINE OF DOCUMENT 2

2.0 *PF*PR DATA ASSEMBLY AND SUMMARY 2

2.1 DATA POINTS FROM SYSTEMATIC LITERATURE REVIEW 2

2.2 DATA POINTS FROM NATIONAL HOUSEHOLD SURVEYS 2

2.3 DATA SUMMARY 5

2.4 DATABASE FIDELITY CHECKS 5

3.0 ENVIRONMENTAL COVARIATE ASSEMBLY 6

4.0 INTERVENTIONS ASSEMBLY 8

4.1 INSECTICIDE TREATED NETS (ITN) 8

4.2 INDOOR RESIDUAL SPRAYING (IRS) 11

4.3 ARTEMISININ BASED COMBINATION THERAPY (ACT) 12

5.0 LATENT GAUSSIAN PROCESS MODEL 12

5.1 OUTLINE 12

5.2 DATA TRANSFORMATIONS AND ADJUSTMENTS 13

5.3 LATENT GAUSSIAN MODEL FORMULATION 14

6.0 ENSEMBLE MODEL FOR CLINICAL INCIDENCE 22

7.0 REFERENCES 24

8.0 DATA ACKNOWLEDGEMENTS 27

1.0 Outline of Document

In this supplementary document we outline the methods and data used to model *Plasmodium falciparum* parasite rate (*Pf*PR) and clinical incidence across Africa from 2000 to 2015. In section 2 we present a summary of the *Pf*PR database and processing procedures applied to the data prior to modelling. In section 3 we present a summary of the covariate selection procedures. In section 4 we outline the data collection and models for intervention coverage. In section 5 we present the latent Gaussian spatio-temporal model for mapping *Pf*PR across Africa and finally, in section 6, we present our predictive ensemble approach to translating *Pf*PR into estimates of clinical incidence.

2.0 *Pf*PR Data Assembly and Summary

2.1 Data points from systematic literature review

Until recent years, the Malaria Atlas Project *Pf*PR database[1,2] was composed primarily of geo-positioned community-based survey measurements of *Pf*PR identified through periodic literature searches from published data sources and direct communication with malaria specialists for unpublished measurements of *Pf*PR.

The methodology used for these data searches is provided in detail in previous MAP publications[1-4]. In brief, exhaustive literature searches have been carried out periodically between March 2005 and May 2015 to identify reported measurements of community-level *Pf*PR. Measurements of *Pf*PR were included in the MAP database according to rigorous inclusion criteria, and subsequently included in this analysis if conducted in Africa after 1995 (see Table 1 for inclusion criteria). In total, 27,573, spatially and temporally unique *Pf*PR observations valid for inclusion in mapping were yielded from these systematic reviews.

2.2 Data points from national household surveys

Data availability from cross-sectional household surveys has rapidly risen within the last decade, as shown in Figure 1, which highlights the overall growth in data (georeferenced points from survey data, published literature and communications with malaria researchers) through time.

The primary source of household survey data is the Demographic and Health Surveys (DHS) Program, a USAID funded organisation that collects nationally representative health and socioeconomic information from national household surveys in over 90 countries worldwide. African national surveys with blood-based malaria testing were downloaded from the DHS Program website (www.dhsprogram.com/). In total, 28 geo-referenced DHS Program surveys conducted in African countries tested for *P. falciparum* prevalence in children under 5 years of age (as of 18th May 2015).

Table 1. Inclusion criteria for geo-referenced *Pf*PR observations from literature for use in mapping.

Inclusion criterion	Criteria for inclusion in MAP database	Criteria for inclusion in 2000-2015 African *Pf*PR mapping
Location	Global	Africa only
Time of survey	Post-1984	Post-1995
Sample size	>0	No change
Sampling method	Random, community based	No change
Spatial duplicate time window	>3-6 months	No change
Numerator/denominator	Required	No change
Age groups sampled	Any, but age group must be specified	No change
Spatial coverage	Points/wide-areas preferred	No change

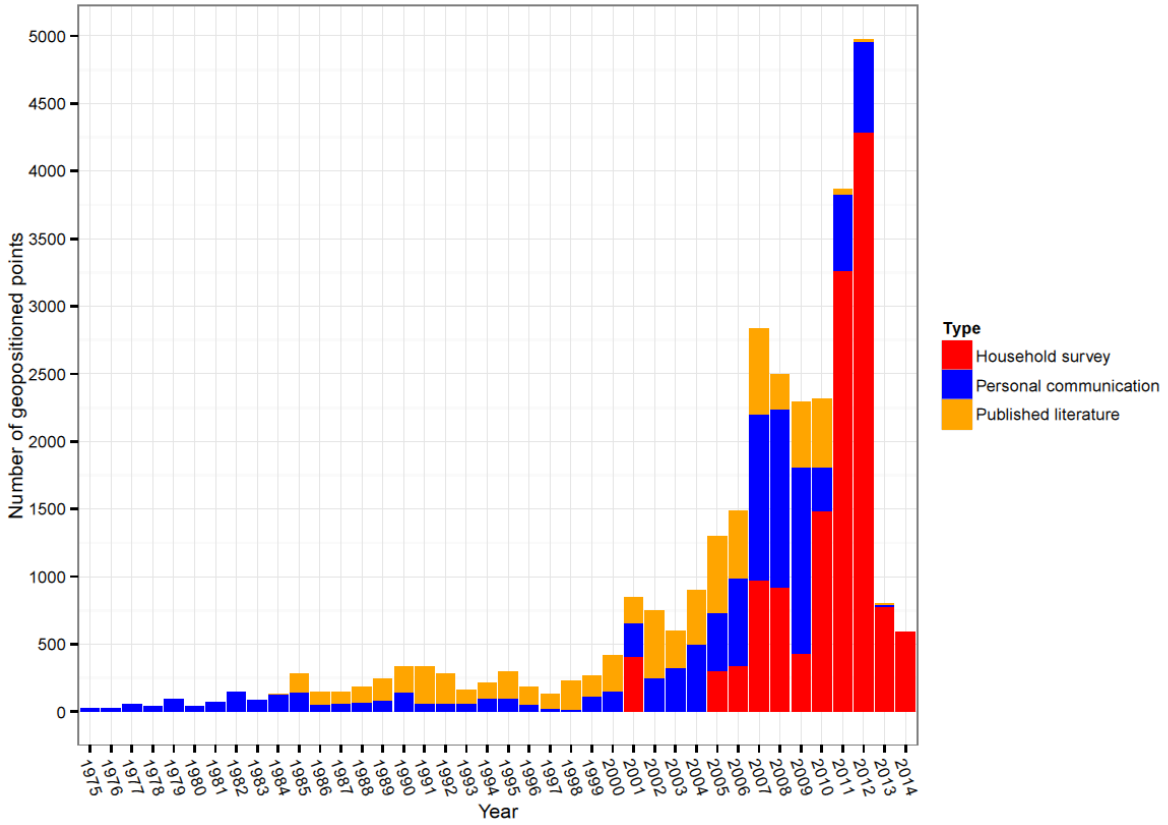

Figure 1. Growth in the availability of household survey data and georeferenced malaria measurements through time.

Table 2. Cross-sectional nationally representative household surveys used in mapping

Country	Survey Year(s)	Source	Number of geo-positioned clusters	Number of individuals	Demographics
Angola	2006-2007	DHS Program	115	2658	Children <5 years; Women 15-49 years
Angola	2011	DHS Program	228	3323	Children <5 years
Benin	2011-2012	DHS Program	735	3791	Children <5 years
Burkina Faso	2010	DHS Program	541	5741	Children <5 years
Burundi	2012	DHS Program	200	3722	Children <5 years
Cameroon	2011	DHS Program	576	6620	Children <5 years
Cote d'Ivoire	2011-2012	DHS Program	341	3801	Children <5 years; Women 15-49 years
Democratic Republic of the Congo	2013-2014	DHS Program	488	7503	Children <5 years
Ghana	2011	UNICEF MICS	775	4352	Children <5 years
Guinea	2012	DHS Program	300	3215	Children <5 years
Liberia	2009	DHS Program	150	4968	Children <5 years
Liberia	2011	DHS Program	150	3207	Children <5 years
Madagascar	2011	DHS Program	266	6827	Children <5 years
Madagascar	2013	DHS Program	274	6232	Children <5 years
Malawi	2012	DHS Program	140	2121	Children <5 years
Mali	2010	DHS Program	106	1716	Children <5 years
Mali	2012-2013	DHS Program	413	5707	Children <5 years
Mozambique	2011	DHS Program	603	4895	Children <5 years
Namibia	2009	Namibia MoH	120	1142	Children <5 years
Nigeria	2010	DHS Program	239	5157	Children <5 years
Rwanda	2007-2008	DHS Program	246	5948	Children <5 years; Women 15-49 years
Rwanda	2010-2011	DHS Program	492	12004	Children <5 years; Women 15-49 years
Senegal	2008-2009	DHS Program	317	4139	Children <5 years
Senegal	2010-2011	DHS Program	383	4603	Children <5 years
Senegal	2012-2013	DHS Program	200	7321	Children <5 years
Sudan	2005	Sudan NMCP	106	8858	All ages
Sudan	2009	Sudan NMCP	287	21164	All ages
Sudan	2012	Sudan NMCP	256	21988	All ages
Swaziland	2010	DHS Program	460	4306	Children <5 years
Tanzania	2007-2008	DHS Program	474	6457	Children <5 years
Tanzania	2011-2012	DHS Program	572	7372	Children <5 years
Togo	2013-2014	DHS Program	329	3,888	Children <5 years
Uganda	2009	DHS Program	170	4011	Children <5 years

The DHS surveys were aggregated to cluster level (a geo-positioned centroid with approximately 25 households associated with each cluster). To protect the identity of surveyed individuals, these clusters are displaced by up to 2km for urban clusters and 5km for rural clusters (with a randomly selected 1% of rural clusters displaced by up to 10km). *Pf*PR at each cluster was calculated from the number of children who received a diagnostic test and, of those, the number of children who tested positive. *Pf*PR (recorded as the number positive and number examined), geo-position, source, urban/rural definitions, age range of individuals, survey dates and diagnostic method were then extracted from each survey at a cluster level and stored in a custom built database in a standardised format.

In addition to DHS Program surveys, other organisations now collect and distribute cross-sectional, nationally representative measurements of cluster malaria prevalence. These include (i) UNICEF Multiple Indicator Cluster Surveys (UNICEF MICS) (www.childinfo.org/mics_available.html) which incorporated blood parasitemia testing in the most recently completed round of surveys (MICS4), and (ii) Health Ministries/National Malaria Control Programmes in malaria endemic countries. In total, five additional non-DHS Program surveys were collected and aggregated using a similar protocol to the DHS Program surveys. The resulting 31 surveys were included in mapping, resulting in an additional 198,757 malaria measurements from individuals across 11,052 geo-positioned sites, and are listed below in Table 2.

2.3 Data summary

A total of 27,573 geo-referenced points from literature searches, personal communications and household surveys were assembled across 43 African countries spanning a time range from 1995 to 2014 (Figure 2).

2.4 Database fidelity checks

Before use in modelling, the database was checked for inconsistencies and errors that could have occurred during data entry. These data checks remained consistent with those used in previous iterations of *P. falciparum* mapping by MAP and include error-checking the fields describing the study area (area type, geographical coordinates, and urban or rural definitions) and those providing specific information about the survey (month and year of start and end of the survey, age range of study population, number examined and positive for P. falciparum, and diagnostic method used). Geo-positioned locations were also checked to ensure the points fell within the borders of the country in which the survey was conducted. Finally, spatio-temporal duplicate points (where observations were reported in the same location within less than three months of each other and had identical counts of both surveyed individuals and those testing positive for *Pf*) were removed, and pairs of survey sites within 1km of each other were corrected to the same unique identifier if they corresponded to the same location.

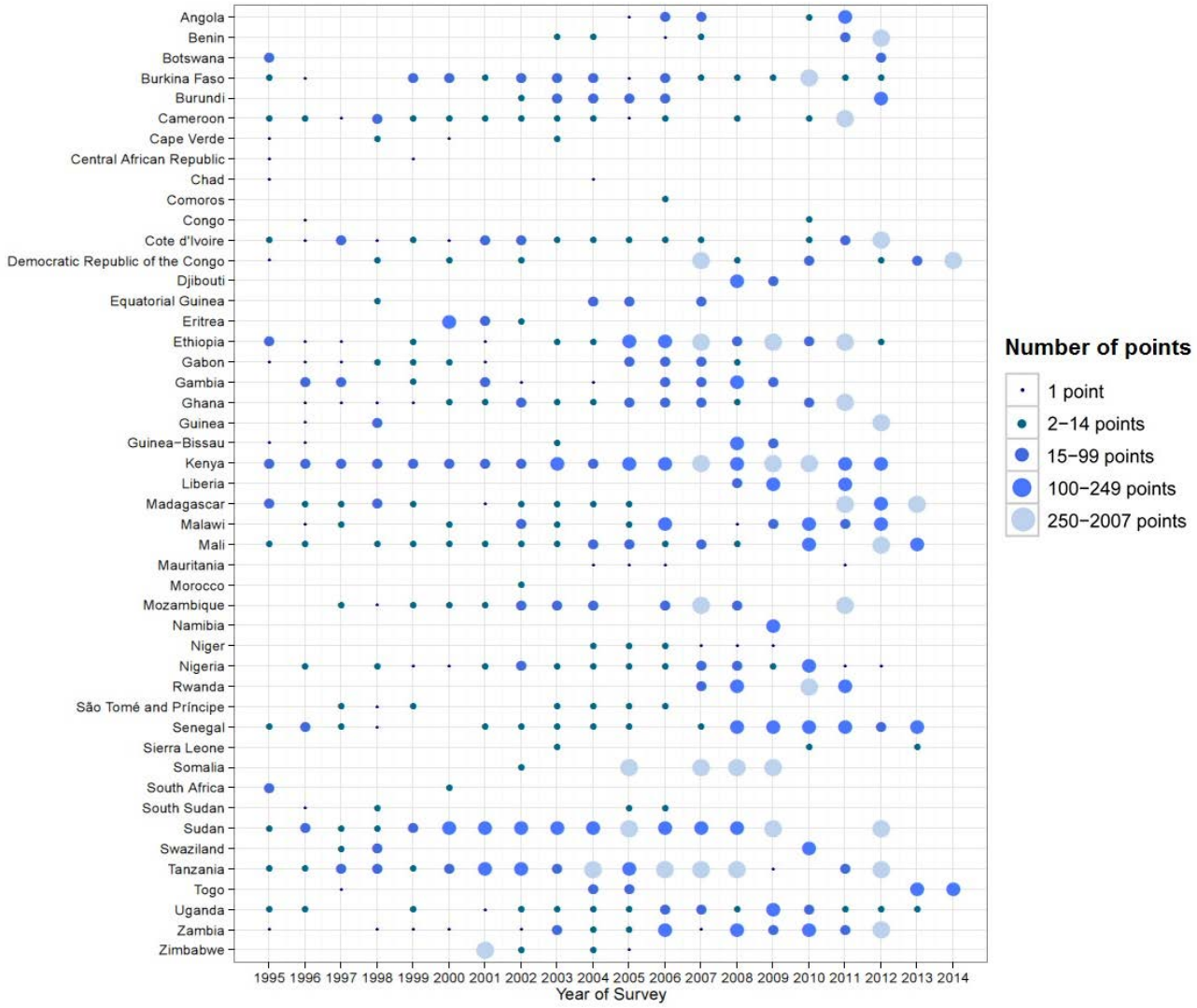

Figure 2. Summary of geo-referenced datapoints included in modelling, stratified by country and year.

3.0 Environmental Covariate Assembly

The environmental covariates (i.e., independent variables) used in this research consisted of raster layers that spanned all of Africa at a 2.5 arc-minute (~5 km x 5 km) spatial resolution. The covariates ultimately used in the *Pf*PR model were chosen via a rigorous variable selection process that is described in Weiss et al. 2015[5]. This variable selection approach began with an exhaustive literature review that identified the key variables used within past malaria mapping endeavours. Raster datasets matching or approximating the variables identified in the literature review were then acquired or produced, and wherever possible dynamic versions (i.e., temporally varying products) were utilized to

support the temporal aspect of the analysis. The list of covariates examined was augmented with additional datasets hypothesized to affect *P. falciparum* vector ecology and transmission. The majority of the raster covariates were derived from high temporal resolution satellite images that were first gap-filled[6] to eliminate missing data resulting primarily from persistent cloud cover over equatorial forests, and then aggregated to create dynamic covariates for every month throughout the study period (2000-2015). The full set of basis covariates is shown in Table 3.

Table 3. Initial datasets explored in the variable selection process and subsequently leveraged into a set of more than 55 million potential covariates.

Variable Class	Variable(s)	Source	Type
Temperature	Land Surface Temperature (daytime, night-time, and diurnal-flux)[7]	MODIS Product	Dynamic Monthly
Temperature Suitability	Temperature Suitability for *Plasmodium falciparum*[8]	Modelled Product	Dynamic Monthly
Precipitation	Mean Annual Precipitation[9]	WorldClim	Synoptic
Vegetation Vigour	Enhanced Vegetation Index[10]	MODIS Derivative	Dynamic Monthly
Surface Wetness	Tasselled Cap Wetness[11]	MODIS Derivative	Dynamic Monthly
Surface Brightness	Tasselled Cap Brightness[11]	MODIS Derivative	Dynamic Monthly
IGBP Landcover	Fractional Landcover[12]	MODIS Derivative	Dynamic Annual
IGBP Landcover Pattern	Landcover Patterns[12]	MODIS Derivative	Dynamic Annual
Terrain Steepness[13]	Slope Angle & Slope Angle Thresholds	SRTM Derivatives	Static
Topographically Redistributed Water[13]	Flow Accumulation & Topographic Wetness Index	SRTM Derivatives	Static
Elevation	Digital Elevation Model[14]	SRTM	Static
Human Population	AfriPop[15] ,GRUMP, and GPW[16]	Modelled Products	Dynamic Annual
Infrastructural Development	Accessibility[17] to Urban Centres and Night-time Lights	Modelled Product and VIIRS	Static
Moisture Metrics	Aridity and Potential Evapotranspiration[18]	Modelled Products	Synoptic

The variable selection procedure then leveraged the set of covariates through the use of spatial and temporal summarizations, temporal anomalies (i.e., deviations from average conditions), temporal lags, non-linear transformations, and bivariate interactions. The result was an effective dataset size of

more than 55 million covariates, which was subsequently reduced to just 20 covariates using a sequence of steps that maximized predictive strength, parameter stability, and stationarity, while minimizing collinearity. The resulting covariates produced a substantial improvement over those used in previous *Pf*PR mapping endeavors[2], as determined using out of sample validation. A secondary goal of the variable selection process was to assess the utility of covariates for use in dynamic *Pf*PR models. To this end, the analysis revealed that the strongest predictor variables tended to be interaction terms between dynamic and synoptic variables (i.e., summarized products derived from many years' worth of data), which suggest that the interplay between long-term, "normal" conditions and dynamic conditions fluctuating at monthly scales is key for characterizing *Pf*PR in Africa.

4.0 Interventions Assembly

4.1 Insecticide treated nets (ITN)

ITN use, defined as the proportion of a population sleeping under an ITN the previous night, has been shown previously to impact malaria transmission, infection prevalence, and mortality. In this section we describe the data and modelling protocols that are used to estimate ITN use at a 5km by 5km resolution.

4.1.1 ITN Data acquisition and summary

We identified and obtained data for the ownership and use of insecticide treated nets from geo-located household surveys conducted in malaria endemic Sub-Saharan African countries since 2000, including demographic health surveys (DHS), malaria indicator surveys (MIS), multiple cluster surveys (MICS), AIDS indicator surveys (AIS), and a malaria and anaemia prevalence survey (EA & P). The number of ITNs, number of individuals that slept in the surveyed households the night prior to the survey, and the number of individuals that slept under an ITN the night prior to the survey were aggregated at the cluster and household level from 61 national surveys from 30 countries collected from 2003 to 2014. The timing, number, and size (i.e., number of clusters and households) of the surveys are summarised in Figure 3.

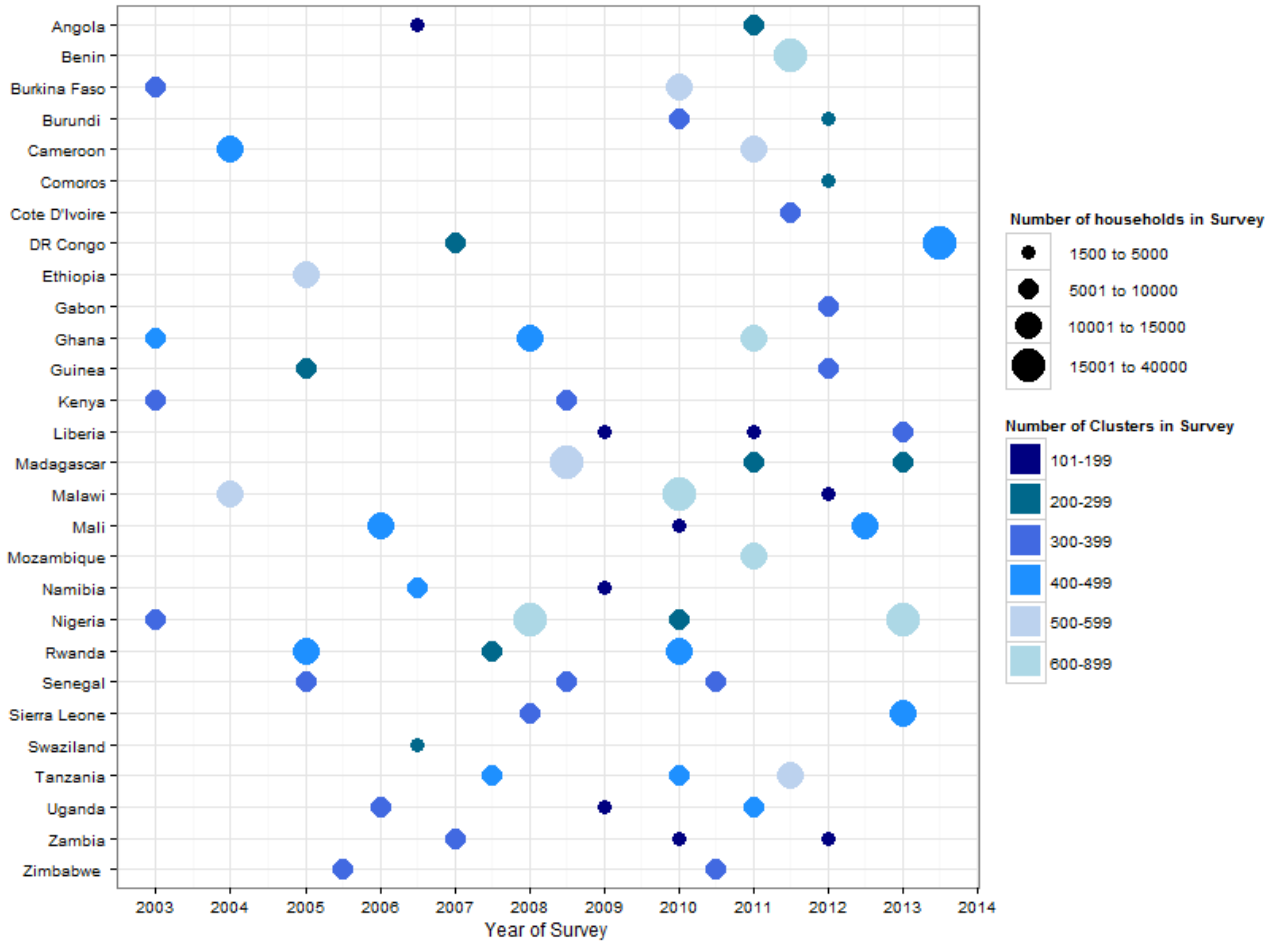

Figure 3. Geo-referenced surveys reporting on ITN coverage included in modelling, stratified by country and year.

4.1.2 Data processing

The DHS surveys provided information on an individual household and cluster/EA level scale. Estimates for ITN use were calculated from the household level as the proportion of individuals sleeping under a net (P_u) out of the total number of individuals that slept in the given household (P). Defining for a given country (c), sets of h households, and s geopositioned clusters. ITN use at a given cluster was therefore calculated as:

$$\lambda_{use,s,t} = \sum_{i=h\in s} P_{u,i} \Big/ \sum_{i=h\in s} P_i \qquad (1)$$

Estimates of ITN access were calculated from the household level, using the definition of access as one net between two people[19], as the proportion of individuals with access to a net (P_a) out of the total number of individuals that slept in the given household (P_i). The calculation for ITN access at a given cluster is:

$$\lambda_{acc,s,t} = \max\left[\sum_{i=h\in s} P_{a,i}, \sum_{i=h\in s} P_i\right] \Big/ \sum_{i=h\in s} P_i \quad (2)$$

The max statement sets an upper bound on the number of individuals with access to the number sleeping within the household. For both $\lambda_{acc,s,t}$ and $\lambda_{use,s,t}$ the time (t) is calculated as the average of the sampling times in $h \in s$. It should be noted that while $\lambda_{acc,s}$ and $\lambda_{use,s}$ are defined above as a rate they could also be represented as binomial variables by splitting the numerator and denominator.

For both $\lambda_{acc,s}$ and $\lambda_{use,s}$ we aggregated data (summing the binomial counts) that fell within the same geographical pixel and the same temporal quarter (the temporal resolution of our analysis). We found that this aggregation did not have significant effects on the model prediction, but did help in model fitting and computational speed due to data size reduction.

4.1.3 Modelling ITN coverage - overview

We developed a Bayesian compartmental model[19] that takes data from manufacturer, NMCP (national malaria control program), and survey sources, and uses these data to model the volume of nets within each country, on a per-capita-at-risk basis, through time. From these estimates of nets per-capita we developed a truncated Poisson model to estimate indicators on ownership, including access, with very high precision. However, we were not able to model use using the same Poisson model and therefore, after recognizing a strong linear relationship between access and use, simply calculated use as a linear function of access. While this linear model was good at predicting the national-level relationship between access and use, it failed to adequately capture subnational deviations. Therefore we refined our estimates by building accurate subnational predictions of net access, which was a more precise method than the simpler linear model approach, and ultimately produced results that corresponded strongly with survey estimates.

4.1.4 Model for sub-national ITN access

We first attempted to model access using a latent Gaussian model (LGM, further explained in section 5) with measurement equation:

$$\lambda_{acc,s,t} \sim \beta X_s + Z_{s,t} + \epsilon \quad (3)$$

where $\epsilon \sim N(0, I\sigma_e^2)$, X_s are static covariates with coefficients β and $Z_{s,t}$ is a spatio-temporal Gauss-Markov random field (GMRF) with Matérn spatial and autoregressive temporal innovations. To avoid potential issues of circularity in later analyses, covariates X_s were chosen, as those *not* used in the *Pf* prevalence models described in section 5.

A challenge that arose in modelling ITN access through the measurement equation above was that the spatial mean of access was extremely non-stationary and varied greatly from country to country, thus

limiting the effectiveness of the raw model. We therefore detrended our access samples using the national means estimated previously[19] ($\mathcal{M}_{s,t}$) . This detrending allowed the overall temporal trend (or mean) in a given country to be correctly calibrated, and left the detrended ITN access observations easy to model across space (through country borders) and time. Conceptually this LGM model determined the spatial pattern of ITN access around the mean. After performing model selection based on out-of-sample validation and information criterion (WAIC[20,21] and DIC[22]) we found that a spatial only GMRF was preferred over the spatio-temporal model. Our final measurement equation for modelling ITN access was therefore:

$$(\lambda_{acc,s,t} - \mathcal{M}_{s,t}) \sim \beta X_s + Z_s + \epsilon \tag{4}$$

4.1.5 Model for use gap

We modelled the use gap, defined as a proportional difference - $\lambda_{gap,s,t} = {(\lambda_{use,s,t} - \lambda_{acc,s,t})}/{\lambda_{acc,s,t}}$

using a LGM with measurement equation:

$$\lambda_{gap,s,t} \sim \beta X_s + Z_{s,t} + T_t + \epsilon \tag{5}$$

where T_t is a nonparametric seasonal trend defined a quarterly intervals with zero mean Gaussian density, and covariance $Q = \tau R$ where τ is the precision parameter and R is the quarterly neighbourhood structure. Unlike our approach for access, after model selection we found that a spatio-temporal GMRF best fitted the use gap data.

4.1.6 Model for use

As discussed in section 4.1.3, after estimating the per-pixel access and use gap, use was calculated as:

$$\lambda_{use,s,t} = \lambda_{gap,s,t}\lambda_{access,s,t} + \lambda_{access,s,t} \tag{6}$$

For ease of notation we will refer to $\lambda_{use,s,t}$ as $\lambda_{s,t}$.

4.2 Indoor residual spraying (IRS)

The annual number of people per country protected by IRS for the years 2000 to 2013 was provided by the World Health Organization (WHO)[19]. The annual IRS coverage was calculated by dividing the number of people protected by the population at risk of malaria, as defined by the proportion of the population at either high or low risk from the World Malaria Report 2013[19]. This calculation assumes that the people protected by IRS are targeted from the population at risk of malaria. For years 2014 and 2015 we used an average of the years 2011,2012 and 2013 for each country. The resulting tabular data was rasterised and used directly as an input into the latent Gaussian model (see section 5).

4.3 Artemisinin based combination therapy (ACT)

To estimate the annual proportion of febrile children treated with an ACT we developed a procedure to address the sparse spatial and temporal nature of the data. We modelled the annual proportion of febrile children treated with ACT (ACT_{feb}) in a country for each year as function of ACT per capita (ACT_{cap}) distributed. In this context ACT_{cap} was considered as proxy of drug availability in each country. A Spearman's correlation test was used to evaluate the correspondence between ACT_{cap} and ACT_{feb} and showed strong correlation (rho=0.66, p<0.01). We modelled the sparse ACT_{cap} data using a LGM with a log normal likelihood (Shapiro-Wilk test, p<0.01) and measurement equation

$$ACT_{cap,c,t,r} \sim f(T_t) + C_c + R_r \quad (7)$$

Where c is a given country, r is a given region, t is the year, $f(T_t)$ is a nonparametric time trend, C_c are country specific random effects, and R_r are region specific random effects. Regions were defined as Eastern, Central, Western, and Central Africa (see UN, http://unstats.un.org/). We assigned Sudan to the Western Africa group because it was the only Northern country in our dataset.

Given the strong correlation between ACT_{cap} and ACT_{feb}, we leveraged the information from the model of ACT_{cap} and used a second LGM to model the sparse ACT_{feb} data. The measurement equation from this second model was:

$$ACT_{feb,c,t,r} \sim f(ACT_{cap,c,t,r}) + C_c + R_r \quad (8)$$

The posterior distribution of both LGMs was estimated using a jackknife approach with 1000 iterations (leaving one data set out per iteration).

5.0 Latent Gaussian Process Model

5.1 Outline

The construction of malaria endemicity maps using model based geostatistics and/or latent Gaussian models[23-25] has been described in detail previously[1,2,26]. In brief, latent Gaussian modelling techniques utilise stochastic Gaussian processes to allow for extremely flexible extensions of generalised linear models[27] while still maintaining a rigorous probabilistic framework (i.e., Bayesian inference). Given temporally dynamic data characterizing environmental conditions (X), interventions ($\mathcal{I}$), baseline parasite rate ($\mathcal{B}$), and residual structural random effects (Z), the LGM model translates discrete survey *Pf*PR observations into a continuous model, $f(\cdot)$, of prevalence through space and time. The model is fully Bayesian and therefore combines information contained in the data (likelihood), with uncertainty in the data generating process (prior), to yield a posterior probability distribution that weights all the available evidence. From this continuous model we can evaluate the posterior

predictive distribution by integrating over the posterior distribution with the parameter uncertainty, resulting in a prediction that spans all of Africa at an approximate 5 km by 5 km spatial resolution.

In this section we describe the steps utilised for modelling continuous *Pf*PR from a database of discrete point estimates. We first describe the transformations applied to the *Pf*PR response data to adjust for age and for diagnostic type, and therefore assist in subsequent computation. We then describe the hierarchical latent Gaussian model formulation used to predict *Pf*PR, highlighting the model specification and fitting.

5.2 Data transformations and adjustments

5.2.1 Raw data

The *Pf*PR dataset used in the MBG model is described in section 2. Survey cluster points from this dataset comprised binomial response $PfPR_A(x_{s,t})$ observations, where A is the age range of the parasite rate observation, s is the geographical location, and t is the average time of sampling at the household level. These binomial observations were defined as the number of *P. falciparum* positive responses from a total sample at each survey location in time.

5.2.2 Age standardisation

Before these observations were used in the MBG model, age standardisation was performed[2,28] to allow survey observations conducted over arbitrary ages ranges to be interpreted as prevalence observations in the epidemiologically relevant and consistent 2-10 years age range ($A = 2 - 10$).

5.2.3 RDT to microscopy conversion

The majority of *Pf*PR data are based on positivity rates determined by either microscopy or rapid diagnostic test (RDT), and the sensitivity and specificity of these approaches are known to differ. We have therefore developed and implemented a method to quantitatively compare and adjust RDT and microscopy-based prevalence estimates to a common standard prior to use in mapping (Mappin et al 2014, in preparation). Briefly, the conversion method uses a Bayesian errors-in-variables approach to acknowledge sampling error in both the dependent and independent variable with an infinite mixture of Gaussians (i.e., a Dirichlet process mixture model[29]) adopted as a highly flexible semi-parametric form for the unknown baseline distribution of the true RDT-derived prevalence. Our hierarchical probit regression model thus takes the form:

$$n_i^{MIC} \sim Binom\left(p_i^{MIC}, n_i^{tot}\right) \quad (9)$$

$$n_i^{RDT} \sim Binom\left(p_i^{RDT}, n_i^{tot}\right) \quad (10)$$

$$\Phi^{-1}\left(p_i^{MIC}\right) = \alpha + \beta * \Phi^{-1}\left(p_i^{RDT}\right) \quad (11)$$

$$\Phi^{-1}\left(p_i^{RDT}\right) \sim N(\mu_i, \sigma_i^2)$$

$$\left\{\mu_i, \sigma_i^2\right\}\left(i = 1, \ldots, n^{obs}\right) \sim F \quad (12)$$

$$F \sim DP\ (G_\Theta, m) \quad (13)$$

$$\alpha, \beta, \Theta, m \sim \pi \quad (14)$$

where n_i^{MIC} represents the number of microscopy-positive counts, n_i^{RDT} the number of RDT-positive counts, n_i^{tot} the sample size, p_i^{MIC} the (unknown) long-run microscopy measured prevalence, and p_i^{RDT} the (regressed) long-run RDT measured prevalence for each of the $i = 1 \ldots n_{obs}$ studies in the complete datset. Following statistical convention $\Phi(.)$ represents the cumulative distribution function of the standard Gaussian, $DP\ (G_\Theta, m)$ represents the Dirichlet process with reference density G_Θ (controlled by the hyper-parameters, Θ), and concentration index m, while π represents a family of priors and hyperpriors chosen for conjugacy with the upper layers. To allow Gibbs sampling of the full posterior we extend the augmented variable method[30] introducing Gaussian latent variables for each positive and negative result for each test (both RDT and microscopy) in each survey. The capacity of the fitted model to predict the predicted microscopy prevalence from the RDT-derived prevalence has been evaluated via leave-one-out cross-validation. The maximum a posteriori conversion formula between RDT and microscopy so-derived was:

$$\Phi^{-1}\left(p_i^{MIC}\right) = -0.24 + 0.95 * \Phi^{-1}\left(p_i^{RDT}\right) \quad (15)$$

5.2.4 Data aggregation

To assist with computation downstream we aggregated data (summing the binomial counts) that fell within the same geographical pixel and the same temporal quarter. We found that this aggregation did not have significant effects on the model prediction, but did help in model fitting and computational speed due to data dimensionality reduction.

5.3 Latent Gaussian model formulation

To simplify notation and aid readability in this section we redefine $PfPr_{s,t,2-10} = y_{s,t}$.

Given the *n* transformed and adjusted $g(y_{s,t}) = PfPr_{s,t,2-10}$ response observations we use a hierarchical LGM with covariates as environmental conditions ($X_{s,t}$), interventions ($\mathcal{I}_{s,t}$), baseline parasite rate ($\mathcal{B}_s$) and random components as *iid* country specific random effects (Y_c), and unobserved structural random effects ($Z_{s,t}$). At a set of prediction locations ($x_{s,t}$), the model can be expressed through the measurement equation:

$$g^{-1}(x_{s,t}) \sim \beta X_{s,t} + \alpha \mathcal{I}_{s,t} + \gamma \mathcal{B}_s + Z_{s,t} + Y_c + \epsilon \quad (16)$$

Where $g(\cdot)$ is the empirical logit[27] and $\epsilon \sim N(0, I\sigma_e^2)$ is the measurement error which is both spatially and temporally uncorrelated. Our response variables are dichotomous random variables, for which the canonical likelihood function is the binomial. Unfortunately models fitted here using a binomial likelihood function grossly misspecified the posterior variance, and the posterior credible intervals did not faithfully reflect the underlying uncertainty in the data (determined from plots of probability integral transforms and Bayesian coverage; see section 7 below). We tried overdispersed models (beta-binomial) and zero inflated models to correct the posterior variance, but these also failed to produce a well-specified model. We therefore opted to use a Gaussian likelihood, where the data was transformed through an empirical logit[23,31] ($g(\cdot)$), which produced well specified posteriors both in terms of calibration of the variance and out of sample prediction of the mean (see section 5.2.5 part 7).

We use a Gaussian process prior on the mean of our Gaussian likelihood, parameterised as a Gaussian Markov random field[32] (GMRF). This Gaussian process allowed for highly flexible stochastic realisations, incorporation of spatio-temporal correlation, and extremely favourable computational properties.

The hyper parameters (θ) that parameterise the likelihood and GMRF prior were defined using probability distributions thus completing the Bayesian hierarchical model formulation.

By combining the Gaussian likelihood, the GMRF prior and the parameter hyperpriors, the hierarchical model was defined as

$$\theta \sim \pi(\theta) \quad (17)$$

$$(x_{s,t} \,|\theta) \sim Gaussian\,(\mu_{s,t|\theta}, Q^{-1}_{x_{s,t}\,|\theta}) \quad (18)$$

$$(y_{s,t}|x_{s,t}, \theta) \sim Gaussian\,(Ax_{s,t} + Y_c, Q^{-1}_{y_{s,t}|x_{s,t},\theta}) \quad (19)$$

where $\mu_{s,t|\theta} = \beta X_{s,t} + \alpha \mathcal{I}_{s,t} + \gamma \mathcal{B}_s + Y_c$, $\theta \in [\sigma_e, \sigma_{iid}, \beta, \alpha, \gamma, \tau, \kappa]$ is a vector of prior probability distributions on the hyper parameters (see section 5.2.5 part 6 for their specification), A is a sparse observation matrix that maps the GMRF to function evaluations at local observations, and $Q^{-1}_{y_{s,t}|x_{s,t},\theta} = I\,{}^{1}\!/_{\sigma_e^2}$. Where I is the identity matrix.

Given the properties of Gaussian distributions[24] we were able to define in closed form the conditional distribution of predictions given the data and hyper parameters:

$$g^{-1}(x_{s,t}|y_{s,t}, \theta) \sim Gaussian(\mu_{s,t|\theta} + Q^{-1}_{x_{s,t}|y_{s,t},\theta}\, A^T Q_{y_{s,t}|x_{s,t},\theta}(y_{s,t} - A\mu_{s,t|\theta}), Q^{-1}_{x_{s,t}|y_{s,t},\theta}) \quad (20)$$

where $Q^{-1}_{x_{s,t}|y_{s,t},\theta} = Q_{x_{s,t|\theta}} + A^T Q_{y_{s,t}|x_{s,t},\theta} A$. Equation 12 provides the conditional expectation or mean for a prediction location given the data and hyper parameters. Given the GMRF prior the conditional in equation 12 is also sparse[33], which allows us to sample individual realisations in a

computationally efficient manner, and thereby allows for aggregations to different scales while keeping the correct marginal variances[34].

We now describe each component of the measurement equation (equation 8) in turn.

5.3.1 $\beta X_{s,t}$ - The covariate component

Here $X_{s,t}$ is a matrix of *20* by *n* covariates intersected for each $y_{s,t}$ observation, and β is a coefficient vector. The selection of these covariates is described briefly in section 3 and readers are directed to Weiss et al 2015[5] for a complete description.

5.3.2 $Z_{s,t}$ - The spatio-temproal covariance function for structured random effects

$Z_{s,t}$ can be thought of as a state process, and is assumed to be a spatio-temporal Gaussian process that is correlated in space by a Matérn covariance function, and in time by first order autoregressive dynamics. The Matérn spatial component is represented through a GMRF as

$$w_s \sim N(0, Q_s) \tag{21}$$

where the sparse precision matrix Q_s is the sparse finite element solution to the stochastic partial differential equation[33], and

$$(k^2 - \Delta)^{\frac{\alpha}{2}}(\tau x(s)) = \varepsilon(s) \tag{22}$$

where Δ is the Laplacian, k is the spatial scale/range parameter, τ controls the variance, α is the spatial smoothness parameter (fixed at $\alpha = 2$), and $\varepsilon(s)$ is the spatial white noise process. *s* is defined on a spherical manifold in Cartesian $\mathbb{R}^3$. For more details see Lindgren et al 2011[33].

Temporal correlation is modelled by first order auto regressive dynamics as $w_t = \phi w_{t-1}$, which yields the GMRF $w_t \sim N(0, Q_t)$.

Combining these two GMRFs into a joint spatio-temporal field is achieved through a Kronecker product of the spatial and temporal precision matricies: $Q_{s,t} = Q_t \otimes Q_s$ where $Q_{s,t}$ is a spatio-temporal precision matrix[35]. The spatio-temporal GMRF prior in the measurement equation is therefore defined as $Z_{s,t} \sim Gaussian(0, Q_{s,t})$.

5.3.3 $\gamma \mathcal{B}_s$ - the baseline parasite rate component

The idea of evaluating the baseline parasite rate was to establish a "fundamental niche" of malaria prevalence that characterizes the stable parasite rate across all of Africa given no interventions or changes in environmental and socioeconomic conditions. This approach has been well established in disease ecology literature[36-38]. The baseline parasite rate is crucial for estimating the change in parasite rate through time, as the baseline parasite rate should equal the current parasite rate in the absence of other changes (e.g., changing climatic patterns, anti-malarial interventions, or unobserved but

correlated changes). This is reflected in the measurement equation (equation 15) where the current parasite rate at any time in space is the same as the baseline parasite rate for a given geographic location given no change in the terms associated with temporally varying covariates (shown in red).

$$g^{-1}(y_{s,t}) \sim \beta X_{s,t} + \alpha \mathcal{I}_{s,t} + \gamma \mathcal{B}_s + Z_{s,t} + Y_c + \epsilon \quad (23)$$

Given this conceptual dependency in the measurement equation, deviations of the parasite rate are then described through the (1) environmental and socio-economic covariates, which determine fluctuations (both seasonally and long term) through time, (2) interventions (ITN, IRS, and ACT), and (3) unobserved yet correlated temporal and spatial patterns (determined from the spatio-temporal covariance).

To model the baseline parasite rate $\mathcal{B}_s$ we split the entire $y_{s,t}$ dataset, and created a subset of *k* observations that occurred at spatio-temporal locations with minimal intervention coverage yet high *Pf* (i.e., ITN use less than 7% and an IRS population at risk coverage less than 30%). The *k* subset was then used to define a purely spatial model of *Pf*PR that encapsulated inter- and intra-annual environmental conditions overly many years, thus producing a model for estimating *Pf*PR that respects natural influences on *Pf*PR while masking the influence of interventions. The application of this model produced a synoptic *Pf*PR surface that effectively serves as a counterfactual dataset for the state of *Pf*PR in the absence of ITN, IRS, and ACT use. The measurement equation used was:

$$\mathcal{B}_s \sim \beta X_s + Z_s + \epsilon \quad (24)$$

where X_s are the environmental covariates for locations *s* in the year 2000, and Z_s is a Matérn GMRF. Out of sample validation and visual inspection showed a large degree of robustness to these thresholds (within sensible variations).

5.3.4 $\alpha \mathcal{I}_{s,t}$ - the interventions component

In our model we include three interventions: (a) insecticide treated bed nets (ITN,λ) (b) indoor residual spraying (IRS, δ) and (c) artemisinin based combination therapy (ACT, η). The generation of these three covariates that comprise the 3 x *n* matrix $\mathcal{I}_{s,t}$ is described in section 3. We will describe the modelling of each of these terms in turn:

5.3.4.1 Insecticide treated bed nets (ITN,λ)

For ITNs, λ due to the richness of the covariate, and following from well developed mathematical models[39,40] we recognised that it also essential to model the dependency on λ contingent on baseline parasite rate and the underling ITN coverage. Additionally we took a moving average of λ to describe the long term effect of ITNs, this average was defined as a four year moving average[40] $\lambda_{avg} = (\sum_{i=t-3}^{t} \lambda_i)/4$.

We fitted a very large suite of candidate functions to simulations taken from OpenMalaria[41,42] and MAPTools[40] and found the functional forms that both quantitatively and qualitatively best fitted these mathematical models was found as $(\mathcal{B}_s^a - \mathcal{B}_s^b)\lambda_{avg}{}^{c\mathcal{B}_s}$. Model fitting among candidate forms was done using Bayesian regression in Stan[43]. This functional form had the advantage of representing a large number of plausible curves, while being bounded appropriately at 0 and 1 and with good statistical properties throughout the entire range.

Using this functional form we determined which set of coefficients best fit $y_{s,t}$ data as $\lambda_{tans} = (\mathcal{B}_s^{0.4} - \mathcal{B}_s^{20})\lambda_{avg}{}^{1.5\mathcal{B}_s}$ by performing a series of iterative grid searches across a fine range of values of *a*, *b* and *c*, and the best model was selected based upon AIC and out of sample validation mean squared error. Finally we used the transformed ITN data within our LGM as a linear component, which allows (1) the functional form of the coefficients to vary within the more constrained range and (2) for relevance detection of the ITN effect.

5.3.4.2 Indoor residual spraying (IRS, δ)

As with ITNs described in 4.1, δ was defined as a two year moving average $\delta_{avg} = (\sum_{i=t-1}^{t} \delta_i)/2$ to represent the long-term effects of IRS. However, while ideally the treatment of δ_{avg} would be represented using the same non-linear form as used for λ_{avg}, the combination of national-level δ_{avg} and the lack of interpretability of the indicator (i.e., population covered) meant we used an untransformed δ_{avg} in the LGM.

5.3.4.3 Artemisinin based combination therapy (ACT, η)

Due to the proportional linear effect of ACTs[39] on $y_{s,t}$ no non-linear model was needed, but as with ITNS and IRS, ACTs were modelled through a 2 year moving average $\eta_{avg} = (\sum_{i=t-1}^{t} \eta_i)/2$. Therefore combining all transformations we defined a matrix $\mathcal{I}_{s,t} \in [\lambda_{trans}, \delta_{avg}, \eta_{avg}]$

5.3.5 Country specific random effects Y_c

Country specific random effects, Y_c, where $c \in [s_1, s_2, .. s_l]$ and *l* is the number of pixels in a given country *c*, were included to allow entire countries to deviate from the global mean and allow for subtle differences of effects across country borders. These effects were distributed as *iid* normal random variables as $Y_c \sim N(0, I\sigma_{iid}^2)$.

5.3.6 Prior probability specifications

Prior probabilities on the fixed effect coefficients were specified as Normally distributed

$$\beta, \alpha, \gamma \sim \text{Gaussian } (0,1000) \quad (25)$$

Prior probabilities on the Matérn range and variance parameters were distributed on a log scale using normal distribution as:

$$\log(\tau) \sim \text{Gaussian}(0,10) \tag{26}$$

$$\log(\kappa) \sim \text{Gaussian}(0,1) \tag{27}$$

The autoregressive parameter for the temporal covariance was distributed on a log transformed proportional scale as:

$$\log((1+\phi)/(1-\phi)) \sim \text{Gaussian}(0,0.15) \tag{28}$$

The country specific random effects variance and the Gaussian likelihood variance were both independently distributed log scale by a log gamma distribution:

$$\log\left(\frac{1}{\sigma_{iid}^2}\right), \log\left(\frac{1}{\sigma_e^2}\right) \sim Loggamma(1,5^{-5}) \tag{29}$$

Changes to the prior distributions did not significantly change posterior fits, and specifications using different prior distributions produced nearly the same posterior parameter fits, thus showing a high degree of robustness to prior specifications.

5.4 Fitting and validation of the LGM

Fitting the LGM was done using an integrated Laplace approximation (INLA) of the posterior conducted using the R package INLA[25]. Testing of the INLA algorithm was performed by comparison on smaller subsets fitted using Hamiltonian Markov Chain Monte Carlo (HMCMC[43]), which showed almost exact correspondence.

Posterior validation was performed by calculating cross validation probability integral transforms (PIT) and five-fold out of sample cross validation. PIT was defined as:

$$PIT_i = \int \mathbb{P}(Y_i \leq PfPr_i | PfPr_{-i}, \theta)\mathbb{P}(\theta | PfPr_{-i})\mathrm{d}\theta \tag{30}$$

The PIT in Equation 30 links actual Pf*Pr* observations relative to the percentiles of their predicted distributions. Given a set of observations $x_1,..,x_n$ with corresponding cumulative predictive distributions $F_1,..,F_n$, the empirical distribution of $F_1(x_1),..,F_n(x_n)$ can be compared against a unit uniform distribution. Therefore, if a sequence of predictive densities coincides with the true data generating process the PITs will be distributed as a unit uniform distribution[44]. Essentially the PIT asks the question "could the fitted model reproduce the data?" Further information on the calculation of the PIT in the INLA framework are describe elsewhere[45]. It should be noted that in practice the PIT values are not always exactly uniform, although convergence is nearly assured as the sample size tends to infinity. Therefore, odd PIT values resulting in u-shaped, nshaped, or skewed distributions

point to a miscalibrated posterior where as those which are approximately uniform point to a well-calibrated posterior with good Bayesian coverage.

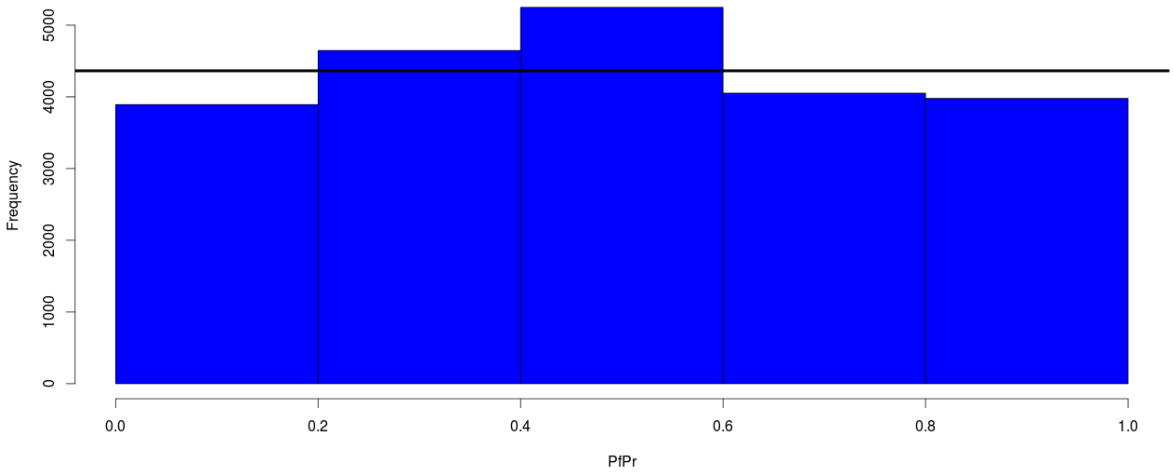

Figure 4. PIT values comparing the data observed values to the cumulative predictive densities. If these two distributions match the data generating process coincides with the predictive distributions and the resulting distribution is approximately uniform.

In addition to calculating PIT values (figure 4) which provide a rigorous evaluation of the posterior predictive distribution we also performed conventional five-fold out of sample validation[46] (figure 5). In accordance with current best practices[47] we randomly partitioned our data into five non overlapping subsets (testing sets) and ran five models on the remaining data (training sets). We then evaluated the correlation and coefficient of determination (R-squared), the mean absolute error, and the mean squared error. Where we had cross sectional national surveys we also compared the average predicted parasite rate to the actual survey rate.

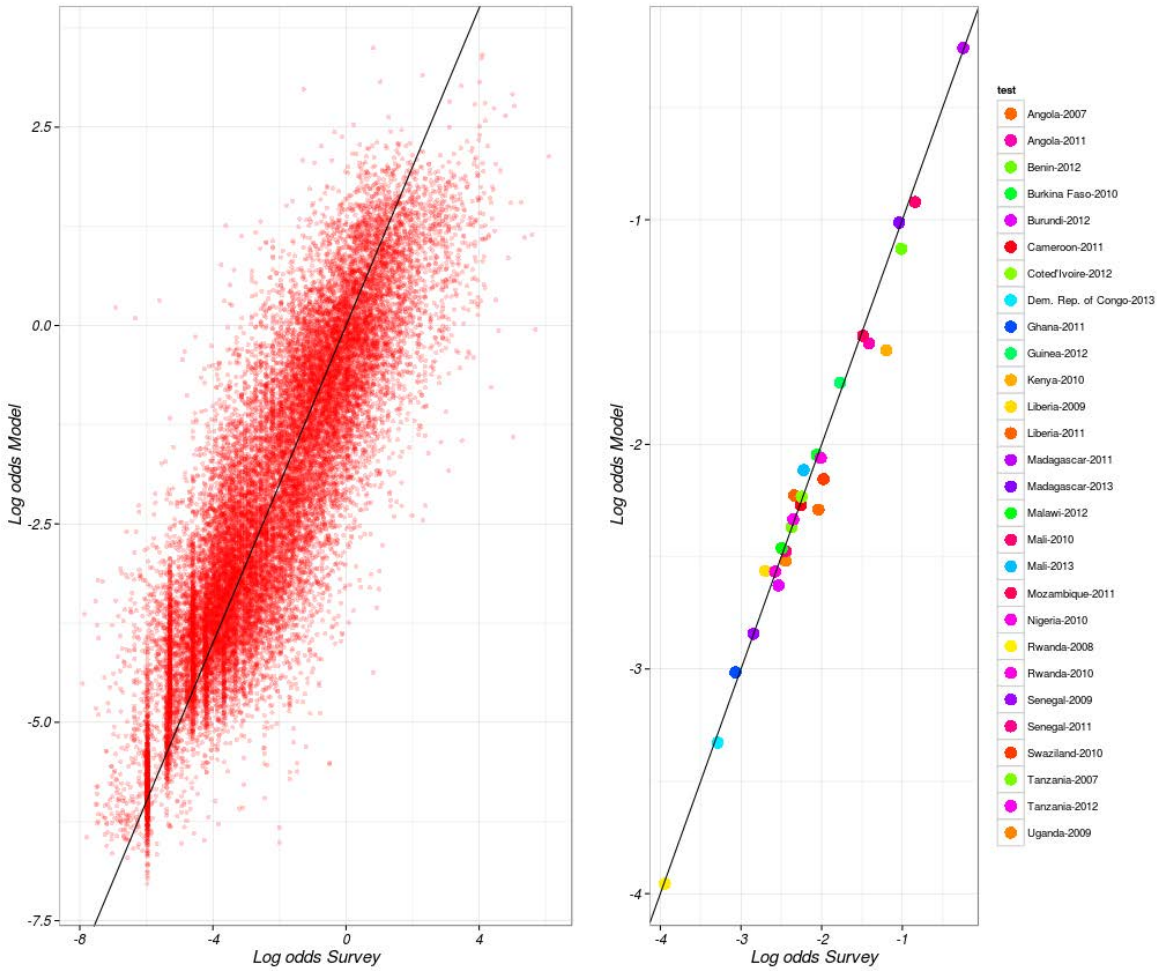

Figure 5. Out of sample validation results at a point level (right) and aggregated survey level (left). Results are displayed in logit (log odds) space as this was the space modelling was performed over.

The correlation and coefficient of determination were 0.87 and 0.75 respectively and the mean absolute error and mean squared error were 9% and 2% respectively. These values indicated a high degree of out of sample predictive accuracy.

5.5 Conditional simulations

Realisations from the fitted LGM were created using the conditional distribution in Equation 12. For a given set of joint parameters $\theta_k \in [\beta, \alpha, \gamma, \tau, \kappa, \phi, \sigma^2_{iid}, 'sigma^2_e]$ a realization from the LGM is evaluated from the conditional distribution as:

$$g^{-1}(x_{s,t}|y_{s,t},\theta)_k \quad (31)$$
$$= \frac{\sum_{l\in[1,..,12]} Gaussian(\mu_{s,t,l|\theta_k} + Q^{-1}_{x_{s,t}|y_{s,t},\theta_k} A^T Q_{y_{s,t}|x_{s,t},\theta_k}(y_{s,t} - A\mu_{s,t|\theta_k}), Q^{-1}_{x_{s,t}|y_{s,t},\theta_k})}{\sum_{l\in[1,..,12]} l}$$

Where l is the month, which is used to incorporate the monthly variation in the dynamic covariates when predicting at a yearly interval t. To incorporate the temporal uncertainty, all years were predicted simultaneously providing a full conditional realization across the entire spatio-temporal range. In total we generated $k = [1,..100]$ samples, each spanning the whole spatio-temporal range

6.0 Ensemble Model for Clinical Incidence

Given the prohibitive cost of active case detection (ACD) as a means to directly monitor the clinical incidence rate of *Plasmodium falciparum* malaria on large scales, recent efforts towards burden enumeration have focussed on identifying a functional relationship between 2-10 y/o prevalence and population-wide incidence as a means to transform cartographic prevalence surfaces to approximate incidence maps[1,48,49]. The latest generation of micro-simulation models, in which entomological inoculation and the course of infection are followed stochastically at the level of individual hosts, offer a sophisticated means to infer this relationship subject to our current epidemiological understanding of the malaria parasite. As no consensus yet exists as to the exact model structure required to accurately represent the observed transmission dynamics, we developed an ensemble modelling approach to constrain the prevalence-incidence relationship with a combination of three contemporary micro-simulation codes (OpenMalaria[41,42], the EMOD DTK[50,51], and an in-house version of the Griffin et al. model[39,52]) fit against a purpose-built empirical dataset of 26 historic ACD surveys covering a total of 30 unique sites across sub-Saharan Africa[53].

To render the posterior calibration procedure computationally tractable, a functional regression-based model emulator for each micro-simulation code was constructed from a library of 100,000 "noisy" (small population) simulation outputs. That is, we use the Nadaraya-Watson form[54] to predict the 2-10 y/o prevalence, $Pf\mathrm{PR}_{2\text{-}10}$, and age-incidence curve, $I(a)$, belonging to a given input pairing of the Entomological inoculation rate (EIR) seasonality profile, $E(t)$, and model parameter list, θ:

$$\hat{R}[\theta, E(t)](a) = \frac{\sum_{i=1}^{n} [Pf\mathrm{PR}_{2\text{-}10}, I(a)] K(d([\theta, E(t)]_i, [\theta, E(t)])/h)}{\sum_{i=1}^{n} K(d([\theta, E(t)]_i, [\theta, E(t)])/h)} \quad (32)$$

where $d(\cdot,\cdot)$ represents a suitable metric distance between points in the functional input space, $K(\cdot)$ denotes a positive definite weighting kernel, and h the associated bandwidth. Simulation from the emulated posterior given our observational dataset was achieved via a pseudo-marginal MCMC sampling scheme[55] with a negative binoimal likelihood function adopted to allow for over-dispersion in the observed incidence counts in addition to a survey-specific random effects term.

Age-, seasonality-, and treatment-structured prevalence-incidence curves were drawn from the posterior predictive distributions of each calibrated emulator and combined into a single ensemble model using a bespoke weighting scheme based on the M-posteriors algorithm[56] The latter, in which two- and three-way agreements between calibrated models are automatically favoured, being preferred over either Bayesian model averaging (overly prior-sensitive) or a raw uniform combination (overly conservative) for our purposes. With the six way structuring of prevalence-incidence curves so produced we seek to improve on the precision of our burden estimates through a stratified sampling approach taking into account the available information concerning variations in the local demography, transmission conditions, and standards of medical service provision across the African continent.

7.0 References

1 Hay, S. I. *et al.* A world malaria map: *Plasmodium falciparum* endemicity in 2007. *PLoS Medicine* **6**, e1000048, (2009).

2 Gething, P. W. *et al.* A new world malaria map: *Plasmodium falciparum* endemicity in 2010. *Malaria Journal* **10**, 378, (2011).

3 Hay, S. I., Guerra, C. A., Tatem, A. J., Noor, A. M. & Snow, R. W. The global distribution and population at risk of malaria: past, present, and future. *The Lancet infectious diseases* **4**, 327-336, (2004).

4 Guerra, C. A. *et al.* The limits and intensity of *Plasmodium falciparum* transmission: implications for malaria control and elimination worldwide. *PLoS medicine* **5**, e38-e38, (2008).

5 Weiss, D. J. *et al.* Re-examining environmental correlates of *Plasmodium falciparum* malaria endemicity: a data-intensive variable selection approach. *Malaria journal* **14**, 68, (2015).

6 Weiss, D. J. *et al.* An effective approach for gap-filling continental scale remotely sensed time-series. *ISPRS Journal of Photogrammetry and Remote Sensing*, (2014).

7 Wan, Z., Zhang, Y., Zhang, Q. & Li, Z.-l. Validation of the land-surface temperature products retrieved from Terra Moderate Resolution Imaging Spectroradiometer data. *Remote Sensing of Environment* **83**, 163-180, (2002).

8 Weiss, D. J. *et al.* Air temperature suitability for *Plasmodium falciparum* malaria transmission in Africa 2000-2012: a high-resolution spatiotemporal prediction. *Malaria Journal* **13**, 1-11, (2014).

9 Hijmans, R. J., Cameron, S. E., Parra, J. L., Jones, P. G. & Jarvis, A. Very high resolution interpolated climate surfaces for global land areas. *International journal of climatology* **25**, 1965-1978, (2005).

10 Huete, A., Justice, C. & Van Leeuwen, W. MODIS vegetation index (MOD13). *Algorithm theoretical basis document*, (1999).

11 Lobser, S. E. & Cohen, W. B. MODIS tasselled cap: land cover characteristics expressed through transformed MODIS data. *Int. J. Remote Sens.* **28**, 5079-5101, (2007).

12 Friedl, M. A. *et al.* MODIS Collection 5 global land cover: Algorithm refinements and characterization of new datasets. *Remote Sensing of Environment* **114**, 168–182, (2010).

13 Beven, K. J. & Kirkby, M. J. A physically based, variable contributing area model of basin hydrology. *Hydrologic Science Bulletin* **24**, 43–69, (1979).

14 Farr, T. G. *et al.* The shuttle radar topography mission. *Reviews of geophysics* **45**, (2007).

15 Tatem, A. J., Noor, A. M. & Hay, S. I. Assessing the accuracy of satellite derived global and national urban maps in Kenya. *Remote Sensing of Environment* **96**, 87-97, (2005).

16 Center for International Earth Science Information Network - CIESIN - Columbia University and Centro Internacional de Agricultura Tropical - CIAT: Gridded Population of the World, Version 3 (GPWv3): Population Density Grid. NASA Socioeconomic Data and Applications Center (SEDAC). (Palisades, NY. 2005.).

17 Nelson, A. Travel time to major cities: A global map of Accessibility. (Global Environment Monitoring Unit - Joint Research Centre of the European Commission 2008).

18 Trabucco, A. & Zomer, R. J. Global Aridity Index (Global-Aridity) and Global Potential Evapo-Transpiration (Global-PET) Geospatial Database., (CGIAR Consortium for Spatial Information, 2009).

19 WHO. *World malaria report 2013*. (World Health Organization, 2014).

20 Gelman, A., Hwang, J. & Vehtari, A. Understanding predictive information criteria for Bayesian models. *Statistics and Computing* **24**, 997-1016, (2014).

21 Watanabe, S. Asymptotic equivalence of Bayes cross validation and widely applicable information criterion in singular learning theory. *The Journal of Machine Learning Research* **11**, 3571-3594, (2010).

22 Gelman, A. *et al. Bayesian data analysis*. (CRC press, 2013).
23 Diggle, P. J., Tawn, J. & Moyeed, R. Model *Journal of the Royal* based geostatistics. *Statistical Society: Series C (Applied Statistics)* **47**, 299-350, (1998).
24 Rasmussen, C. Gaussian processes in machine learning. *Advanced Lectures on Machine Learning*, 63-71, (2004).
25 Rue, H., Martino, S. & Chopin, N. Approximate Bayesian inference for latent Gaussian models by using integrated nested Laplace approximations. *Journal of the royal statistical society: Series b (statistical methodology)* **71**, 319-392, (2009).
26 Gething, P. W. *et al.* Climate change and the global malaria recession. *Nature* **465**, 342-345, (2010).
27 McCullagh, P. & Nelder, J. A. *Generalized linear models*. (Chapman & Hall/CRC, 1989).
28 Smith, D. L., Guerra, C. A., Snow, R. W. & Hay, S. I. Standardizing estimates of the *Plasmodium falciparum* parasite rate. *Malaria journal* **6**, 131, (2007).
29 Escobar, M. D. & West, M. Bayesian density estimation and inference using mixtures. *Journal of the american statistical association* **90**, 577-588, (1995).
30 Albert, J. H. & Chib, S. Bayesian analysis of binary and polychotomous response data. *Journal of the American statistical Association* **88**, 669-679, (1993).
31 Stanton, M. C. & Diggle, P. J. Geostatistical analysis of binomial data: generalised linear or transformed Gaussian modelling? *Environmetrics* **24**, 158-171, (2013).
32 Rue, H. & Held, L. *Gaussian Markov random fields: theory and applications*. (CRC Press, 2005).
33 Lindgren, F., Rue, H. & Lindström, J. An explicit link between Gaussian fields and Gaussian Markov random fields: the stochastic partial differential equation approach. *Journal of the Royal Statistical Society: Series B (Statistical Methodology)* **73**, 423-498, (2011).
34 Gething, P. W., Patil, A. P. & Hay, S. I. Quantifying aggregated uncertainty in Plasmodium falciparum malaria prevalence and populations at risk via efficient space-time geostatistical joint simulation. *PLoS Computational Biology* **6**, (2010).
35 Cameletti, M., Ignaccolo, R. & Bande, S. Comparing spatio -temporal model matter in Piemonte. *Environmetrics*, (2011).
36 Elith, J. *et al.* Novel methods improve prediction of species' distributions from occurrence data. *Ecography* **29**, 129-151, (2006).
37 Stevens, K. B. & Pfeiffer, D. U. Spatial modelling of disease using data-and knowledge-driven approaches. *Spatial and Spatio-temporal Epidemiology*, (2011).
38 Bhatt, S. *et al.* The global distribution and burden of dengue. *Nature* **496**, 504-507, (2013).
39 Griffin, J. T. *et al.* Reducing *Plasmodium falciparum* malaria transmission in Africa: a model-based evaluation of intervention strategies. *PLoS medicine* **7**, e1000324, (2010).
40 Smith, D. L., Hay, S. I., Noor, A. M. & Snow, R. W. Predicting changing malaria risk after expanded insecticide-treated net coverage in Africa. *Trends in parasitology* **25**, 511-516, (2009).
41 Smith, T. *et al.* Ensemble modeling of the likely public health impact of a pre-erythrocytic malaria vaccine. *PLoS medicine* **9**, e1001157, (2012).
42 Smith, T. *et al.* Mathematical modeling of the impact of malaria vaccines on the clinical epidemiology and natural history of *Plasmodium falciparum* malaria: Overview. *The American journal of tropical medicine and hygiene* **75**, 1-10, (2006).
43 Carpenter, B. *et al.* Stan: A Probabilistic Programming Language.
44 Gneiting, T., Balabdaoui, F. & Raftery, A. E. Probabilistic forecasts, calibration and sharpness. *Journal of the Royal Statistical Society: Series B (Statistical Methodology)* **69**, 243-268, (2007).
45 Held, L., Schrödle, B. & Rue, H. in *Statistical modelling and regression structures* 91-110 (Springer, 2010).

46 Bishop, C. M. & ligne, S. *Pattern recognition and machine learning*. Vol. 4 (springer New York, 2006).

47 Abu-Mostafa, Y. S., Magdon-Ismail, M. & Lin, H.-T. *Learning from data*. (AMLBook, 2012).

48 Snow, R. W., Guerra, C. A., Noor, A. M., Myint, H. Y. & Hay, S. I. The global distribution of clinical episodes of *Plasmodium falciparum* malaria. *Nature* **434**, 214-217, (2005).

49 Patil, A. P. *et al.* Defining the relationship between *Plasmodium falciparum* parasite rate and clinical disease: statistical models for disease burden estimation. *Malar J* **8**, 186-186, (2009).

50 Wenger, E. A. & Eckhoff, P. A. A mathematical model of the impact of present and future malaria vaccines. *Malar J* **12**, 10.1186, (2013).

51 Eckhoff, P. A. A malaria transmission-directed model of mosquito life cycle and ecology. *Malar J* **10**, (2011).

52 Griffin, J. T., Ferguson, N. M. & Ghani, A. C. Estimates of the changing age-burden of *Plasmodium falciparum* malaria disease in sub-Saharan Africa. *Nature communications* **5**, (2014).

53 Battle, K. E. *et al.* Global database of *Plasmodium falciparum* and P.vivax incidence records, 1985-2013. *Scientific Data* **Accepted**, (2015).

54 Ferraty, F., Van Keilegom, I. & Vieu, P. Regression when both response and predictor are functions. *Journal of Multivariate Analysis* **109**, 10-28, (2012).

55 Andrieu, C. & Roberts, G. O. The pseudo-marginal approach for efficient Monte Carlo computations. *The Annals of Statistics*, 697-725, (2009).

56 Minsker, S., Srivastava, S., Lin, L. & Dunson, D. in *Proceedings of the 31st International Conference on Machine Learning (ICML-14)*. 1656-1664.

8.0 Data Acknowledgements

This study, and the wider work of the Malaria Atlas Project, is critically reliant on the support of the malaria research, policy, and control communities who generously provide access to their valuable malariometric data collected from endemic countries. Here we list those individuals and organizations, organized by country.

Angola

Susana Nery, Dina Gamboa, José Figueiredo, Claudia Videira, MEASURE DHS, Ana Paula Arez, Akiko Matsumoto, João Mário Pedro, António Langa, Assumpta Bou-Monclus, Cristina Mendes, Clara Burgert. CISA Project - Health Research Center in Angola

Benin

Umberto D'Alessandro, Georgia B Damien, Marie-Claire Henry, Florence Migot-Nabias, Alain Nahum, Christophe Rogier

Botswana

Colleen Fraser, Ababio Grace, Musa Mabaso, Thato Motshoge, Giacomo Maria Paganotti, Isaac Kweku Quaye, John Read, Graham Root, Leabaneng Tawe

Burkina Faso

Heiko Becher, Claudia Beiersmann, Diadier Diallo, Amadou Konate, Bocar Kouyaté, Christian Lengeler, Diseases of the Developing World TAU, Olaf Muller, GlaxoSmithKline, André Lin Ouédraogo, Hermann Ouédraogo, Christophe Rogier, Yazoume Ye

Cameroon

Eric Achidi, Kenneth Ndamukong, Maria Rebollo, Peter Uzoegwu, Samuel Wanji

Chad

Soce I Fall

Côte d'Ivoire

Hortense Aka, Renaude J. Amon, Bassirou Bonfoh, Marie-Chantal Cacou, Marie-Claire Henry, Richard F. Hurrell, Benjamin Koudou, Barbara Matthys, Eliézer K. N'Goran, Charlemagne Nindjin, Giovanna Raso, Fabian Rohner, Daniel E. Sess, Kigbafori Silue, Marcel Tanner, Marguerite D. Té-Bonlé, Andreas B. Tschannen, Jürg Utzinger, Penelope Vounatsou, Rita Wegmüller, Michael B. Zimmermann

Democratic Republic of the Congo

Mike Bangs, Mark Divall, Didier Kabing, Astrid Knoblauch, Jolyon Medlock, Steve Meshnick, Janey Messina, Eric Mukomena Sompwe, Edouard Swana, Mirko Winkler

Djibouti

Mouna Osman Aden, Ifrah Ali Ahmed, Christophe Rogier, Ghasem Zamani

Equatorial Guinea

Ana Paula Arez, Estefanía Custodio, Cristina Mendes, Gloria Nseng

Eritrea

Tewolde Ghebremeskel, Joe Keating, David Sintasath

Ethiopia

Cynthia Beall, Estifanos Biru, Peter Byass, Karre Chawicha, Wakgari Deressa, Yeshewamebrat Ejigsemahu, Paul Emerson, Tekola Endeshaw, Amha Gebremedhin, Teshome Gebre, Asrat Genet, Asefaw Getachew, Lemu Golassa, Patricia Graves, Afework Hailemariam, Don Hopkins, Bernt Lindtjørn, Daddi Jima, Ayenew Messele, Aryc Mosher, Jeremiah Ngondi, Frank Richards, Niko Speybroeck, Zerihun Tadesse, Adugna Woyessaa of Addis Ababa University and the Ethiopian Health & Nutrition Research Institute, Delenasaw Yewhalaw, Mulat Zerihun, Trigray Health Bureau

Gabon

Dieudonné Nkoghe, Odile Oukem, Florence Migot-Nabias

Guinea

Mark Divall, Astrid Knoblauch, Mirko Winkler

Guinea-Bissau

Poul-Erik Kofoed, Amabelia Rodrigues, Michael Walther

Kenya

Timothy Abuya, Kubaje Adazu, Willis Akhwale, Victor Alegana, Pauline Andang'o, Fred Baliraine, Nabie Bayoh, Philip Bejon, Simon Brooker, Maria Pia Chaparro, Jon Cox, Meghna Desai, Diseases of the Developing World TAU, Ulrike Fillinger, GlaxoSmithKline, Joana Greenfield, Andrew Githeko, Laura Hammitt, Carol Gitonga, Helen Guyatt, Katherine Halliday, Mary Hamel, Allen Hightower, Susan Imbahale, Chandy John, Elizabeth Juma, Jimmy Kahara, Simon Kariuki, Carolyne Kifude, Charles King, Chris King, Rebecca Kiptui, Feiko ter Kuile, Kayla Laserson, Tjalling Leenstra, Alex Macharia, Hortance Manda, Kevin Marsh, Margaret McKinnon, Noboru Minakawa, Sue Montgomery, Eric Muchiri, Richard Mukabana, Tabitha Mwangi, Miriam Mwjame, Carolyne Ndila, Charlotte Neumann, Ella Nkhoma George Nyangweso, Christopher Nyundo, Christopher Odero, Edna Ogada, Bernard Okech, George Okello, Maurice Ombok, Simon Omollo, Judy Omumbo, Beth Rapuoda, Evan Secor, Shivang Shah Larry Slutsker, Lia Smith Florey, Jennifer Stevenson, Willem Takken, Sophie Uyoga, Juliana Wambua, Vincent Were, John Waitumbi, Shona Wilson, Guofa Zhou, Dejan

Zurovac & the Kenya National Bureau of Statistics, NUITM-KEMRI project (Nagasaki University Institute of Tropical Medicine and Kenya Medical Research Institute)

Liberia

Richard Allan, Kristin Banek, Clara Burgert, MEASURE DHS

Malawi

Adam Bennett, Cameron Bowie, Bernard Brabin, Marian Bruce, Job Calis, Michael Coleman, Thomas Eisele, Timothy Holtz, Gertrude Kalanda, Lawrence Kazembe, Immo Kleinschmidt, David Lalloo, Don Mathanga, Malcolm Molyneux, Kelias Msyamboza, Piyali Mustaphi, Themba Mzilahowa, Kamija Phiri, Paul Prinsen Geerligs, Arantxa Roca-Feltrer, Andrea Sharma, Bertha Simwaka, Rick Steketee, Anja Terlouw, The Innovative Vector Control Consortium

Mali

Amadou Ballo, Sounkalo Dao, Mahamadou Diakite, Diadier Diallo, Alassane Dicko, Diseases of the Developing World TAU, Abdoulaye Djimde, Ogobara Doumbo, Rick Fairhurst, GlaxoSmithKline, Naffet Keita, Ousmane A. Koita, Carole Long; Lansana Sangare, Hamadoun Sango, Issaka Sagara, Mahamadou Sissoko, Ousmane Toure, Manijeh Vafa and Malaria Research and Training Center (MRTC), Department of Epidemiology of Parasitic Diseases, Faculty of Medicine, University of Bamako, Mali

Mauritania

Ba Mamadou dit Dialaw

Mozambique

Pedro Alonso, Michael Coleman, Albert Kilian, Immo Kleinschmidt, Samuel Mabunda, Allan Schapira, MRC South Africa, The Innovative Vector Control Consortium

Namibia

Colleen Fraser, Frank Hansford, John Irish, Richard Kamwi, Stark Katokele, Musa Mabaso, Kudzai Makomva, John Mendelsohn, Bruno Moonen, Benson Ntomwa, Andreas Reich, Christine Theron, Petrina Uusiku

Niger

Jean-Bernard Duchemin

Nigeria

Emmanuel Adegbe, George Ademowo ,Grace Adeoye, Chiaka Anumudu, Ebere Anyachukwu, Samson Awolola, Ebenezer Sheshi Baba, William Brieger, Marian Bruce, , Diseases of the Developing World TAU, Paul Emerson, Emmanuel Emukah, Bayo Fatunmbi, GlaxoSmithKline, Patricia Graves, Celia Holland, Nnaemeka Iriemenam, Zaccheaus Jeremiah, Michael Kaplan, Albert

Kilian, Paddy Kirwan, Kolawole Maxwell, Peter Olumese, Yusuf Omosun, Sola Oresanya, Frank Richards, Peter Uzoegwu

Rwanda

Caterina Fanello, Jean-Bosco Gahutu, Béatrice Gulbis, Alain Kabayiza, Corrine Karema, Frank Mockenhaupt, Alphonse Mutabazi, Alphonse Rukondo

Senegal

Clara Burgert, Oumar Gaye, Sylvia Males, MEASURE DHS, Florence Migot-Nabias, Rick Paul, Badara Cisse, Ibrahim Socé Fall

Sierra Leone

Matthew Burns, Astrid Knolauch, Mirko Winkler

Somalia

Imanol Berakoetxea, Mohammed Borle, Matthew Burns, Waqar Butt, Craig Von Hagen, Abdi Hersi, Grainne Moloney & the Food Security Analysis Unit (FSAU) team, Bruno Moonen, Abdi Noor, Ismail Rage, Tanya Shewchuk & the Ministries of Health of Puntland, Somaliland and the Transitional National Government

South Africa

Karen Barnes, Frank Hansford, Gerdalize Kok, Philip Kruger, Aaron Mabuza, Rajendra Maharaj

South Sudan

Robert Azairwe, Steve Barya, Bill Gueth Kueil, Margaret Lejukole, Charles Agono Mona, Heidi ReidRage, Tanya Shewchuk & the Ministries of Health of Puntland, Somaliland and the Transitional National Government Karen Barnes, Frank Hansford, Gerdalize Kok, Philip Kruger, Aaron Mabuza, Rajendra Maharaj, Ghasem Zamani

Sudan

Mubashar Ahmed, Fatih Malik, Tayseer Elamin El Faki, Bakari Nour, Ibrahim El Hassan, Abdelhameed Elbirdiri Nugad, Alaa Moawia, Khalid Elmardi, Jaffar Mirghani, Ghasem Zamani, Sahar Bakhite, Alnazear Abdalla, Dalin Abdelkareem Altahir, Fazza Munim, Abdullah Sayied Mohammed, A. Omer, Mustafa Dukeen, Jihad Eltaher Sulieman, Tareg Abdelgader, Abdalla Ahmed, Nasruddin Abdul-Hadi, Abdala Sayaid, Samia Seif Murghan, Ali Elamin Nasir, Mohamed Abbas, Limya El Yamani, Salah Elbin Elmubark, Maowia Mukhtar, Tasneem Moawia, Mohamad Tarig.

Tanzania (United Republic of)

Ali Abdullah, Mike Bangs, Jubilate Barnard, James Beard, Michael Beasley, Achuyt Bhattarai, Anders Bjorkman, Bob Black, Teun Bousema, Clara Burgert, Ilona Carneiro, Prosper P Chaki, Daniel Chandromohan, Diseases of the Developing World TAU, Mark Divall, Stefan Dongus, Chris

Drakeley, GlaxoSmithKline, Yvonne Geissbühler, Nicodem J Govella, Francesco Grandesso, Kara Hanson, Deus Ishengoma, Patrick Kachur, Rose Kibe, Gerry Killeen, Samson Kiware, Astrid Knoblauch, Paul Lango, Martha Lemnge, Neil F Lobo, Rose Lusinde, John Lusingu, Alpha D Malishee, Tanya Marchant, Caroline Maxwell, Ben Mayala, Leonard Mboera, MEASURE DHS, Yeromin Mlacha, Bruno Mmbando, Fabrizio Molteni, Daniel Msellemu, Zacharia J Mtema, Frank Mtei, Athuman Muhili, John Owuor, Hugh Reyburn, Tanya L Russell, David Schellenberg, Sunil Sazawal, Masanja Segeja, Method Donald Segeja ,Tom Smith, Jose Sousa-Figueiredo, Thor Theander, Andrew Tomkins, Jacobien Veenemans, Hans Verhoef, Ying Zhou

The Gambia

Onome Akpogheneta, Steve Allen, Sarah Atkinson, Kalifa Bojang, Sian Clarke, David Conway, Umberto D'Alessandro, Chris Drakeley, Sam Dunyo, Malang Fofana, Brian Greenwood, Adam Jagne-Sonko, Cherno Jallow, Ebrima Jarjou, Momodou Kalleh, Steve Lindsay, Karafa Manneh, Ousman Nyan, Margaret Pinder, Eleanor Riley, Judith Satoguina, Lorenz von Seidlein, Sheriffo Sonko, Michael Walther

Togo

Kodjo Morgah, Anja Terlouw

Zambia

Pascalina Chanda, Elizabeth Chizema, Mike Coleman, Mark Divall, Thom Eisele, Lindsey Everett, Aniset Kamanga, Joe Keating, Immo Kleinsmidt, Mulakwa Kamuliwo, Astrid Knoblauch, Sungano Mharakurwa, John Miller, Boniface Mutombo, Eric Njunju, Richard Steketee, Philip Thuma, The Innovative Vector Control Consortium

Zimbabwe

Graham Root, Tim Freeman, Nicholas Midzi, Francisca Mutapi, Ministry of Health and Child Welfare of Zimbabwe